*Doctoral Thesis*

# Energization and Acceleration of Dayside Polar Outflowing Oxygen

**by**

**Sachiko Arvelius**
Swedish Institute of Space Physics
P.O.Box 812, SE-98128 Kiruna, Sweden

ISSN 0284–1703
ISBN 91–7305–963

Ver. 2.0
October 2005

“You scientists are so shy,”...
“You love to hide your light under a bushel basket.
You’d never guess what’s in those articles from the titles.
Einstein’s first work on the Theory of Relativity was called
’The Electrodynamics of Moving Bodies’. No $E$=$mc^2$ up front.”
——————————— *Contact*, C. Sagan.

# Abstract

This thesis deals with energetic oxygen ions (i.e. single-charged atomic oxygen ions, $O^+$) at altitudes higher than 5 Earth radii ($R_E$) and at latitudes above 75 (toward 90) degrees invariant latitude (deg ILAT) in the dayside polar magnetosphere observed by Cluster. The instrument used in this study is CIS (Cluster Ion Spectrometry experiment) / CODIF (a time-of-flight ion COmposition and DIstribution Function analyser), which covers an energy range from $\sim$10 eV up to 38 keV. Cluster detected $O^+$ with energies more than 1 keV (hereafter termed "keV $O^+$"), indicating that energization and/or acceleration process(es) take place in the dayside high-altitude (inside magnetopause) and high-latitude region. These $O^+$ are outflowing (precisely, upward-going along the geomagnetic field lines), and these outflowing keV $O^+$ show a heated (or energized) signature in the velocity distribution as well.

First, outflowing $O^+$ are observed at the poleward cusp and/or the mantle formed a partial shell-like configuration seen in the velocity distribution. Second, the latitudinal distribution of outflowing $O^+$ (most of them have energies less than 1 keV statistically) observed below 7 $R_E$ is consistent with velocity filter effect by the polar convection, while the latitudinal distribution of outflowing keV $O^+$ observed above 7 $R_E$ cannot be explained by velocity filter effect only, i.e. this indicates that additional energization and/or acceleration takes place at higher altitudes in the dayside polar region. Thirdly, a tendency to observe outflowing keV $O^+$ for during different geomagnetic conditions is studied. The keV $O^+$ above 9 $R_E$ is more often for $K_p \geq 5$ rather than for $K_p \leq 3$. However the energy of $O^+$ is not dependent on $ASY/SYM$ indices.

Finally, the dependence on the solar wind conditions is also studied. The energization and/or acceleration of outflowing $O^+$ is controlled by both solar wind moments (except solar wind electric field) and strong southward interplanetary magnetic field (IMF) at the time scale of tens of minutes at only higher altitudes. Further examination shows that solar wind dependence is different at three regions: one is the poleward cusp, another is the low-altitude polar cap, and finally the high-altitude polar cap, combining all the results. There is (a) new energization and/or acceleration process(es) at the high-altitude polar cap. On the other hand, flux enhancement of $O^+$ observed above 5 $R_E$ is also controlled by solar wind moments (e.g. solar wind electric field) and strong southward IMF, however the ionospheric changes play a more important role on the flux enhancement of $O^+$.

**Key words:** Solar wind-magnetosphere interactions; Magnetosphere-ionosphere coupling; $O^+$ energization/acceleration; $O^+$ outflow.

# Acknowledgements

I would like to thank the Swedish Institute of Space Physics (Institutet för rymdfysik, IRF), for offering me the opportunity to take my Ph.D in Kiruna. In Particular I am very grateful to Dr. Masatoshi Yamauchi for advising me to apply for the Ph.D position at IRF in Kiruna, also for advising me on the latest works and this thesis. I also want to thank my supervisor, Professor Ingrid Sandahl, who organized my Ph.D studies, project leader, Professor Rickard Lundin, who gave me a lot of scientific advice, Dr. Hans Nilsson, who collaborated and discussed with me orienting the same goal. My Ph.D work at IRF in Kiruna has been funded by Umeå University and has been supported in general by IRF. Regarding this thesis and the following papers, Lisa Quasthoff-Holmström and Dr. Rick McGregor have checked them out linguistically.

I would like to send my special thanks to my parents, brother and sister. They have known for a long time that I have been fascinated with the 'space' and eager for studying space physics during my teens and twenties. When I got a chance to restart my study "in Sweden", they just encouraged me to earn a degree instead of earning a lot of money. Finally I would like to mention that I have spent a very fruitful time both on Ph.D study and on private life in Kiruna because, for the latter in particular, I have a good husband/colleague/partner in common hobbies, Johan Arvelius, and our precious daughter, 'lilla' Karin.

# Contents

# List of papers

The following papers first-authored by Sachiko Arvelius (former Joko) are included in this doctoral thesis.

## Paper I:

*Shell-like configuration in $O^+$ ion velocity distribution at high altitudes in the dayside magnetosphere observed by Cluster/CIS*,
S. Joko, H. Nilsson, R. Lundin, B. Popielawska, H. Rème, M. B. Bavassano-Cattaneo, G. Paschmann, A. Korth, L. M. Kistler, and G. K. Parks.
*Annales Geophysicae*, 22, 2473–2483, 2004.

## Paper II:

*Statistics of high-altitude and high-latitude $O^+$ ion outflows observed by Cluster/CIS*,
S. Arvelius, M. Yamauchi, H. Nilsson, R. Lundin, Y. Hobara, H. Rème, M. B. Bavassano-Cattaneo, G. Paschmann, A. Korth, L. M. Kistler, and G. K. Parks.
*Annales Geophysicae*, 23, 1909–1916, 2005.

## Paper III:

*Statistical study of relationships between dayside high-altitude and high-latitude $O^+$ ion outflows, solar winds, and geomagnetic activity*,
S. Arvelius, M. Yamauchi, H. Nilsson, R. Lundin, H. Rème, M. B. Bavassano-Cattaneo, G. Paschmann, A. Korth, L. M. Kistler, and G. K. Parks.
submitted to *Annales Geophysicae*, 2005.

The paper below is co-authored by Sachiko Arvelius (Joko) and very close related to this doctoral thesis. However, the contents of this paper is not dealt explicitly in this doctoral thesis, just as one reference.

## Paper IV:

*The structure of high altitude $O^+$ energization and outflows: a case study*,
H. Nilsson, S. Joko, R. Lundin, H. Rème, J.-A. Sauvaud, I. Dandouras, A. Balogh, C. Carr, L. M. Kistler, B. Klecker, C. W. Carlson, M. B. Bavassano-Cattaneo, and A. Korth.
*Annales Geophysicae*, 22, 2497–2506, 2004.

“Y’see, you scientists are too skeptical.”...
“...You always want to check out if a thing is what you call ’true’.
And ’true’ means only empirical, sense data, things you can see and touch.
There’s no room for inspiration or revelation in your world.”
——————————— *Contact*, C. Sagan.

# Chapter 1

# Introduction – Importance of $O^+$ outflow study

Ionospheric plasma outflow into the magnetosphere was studied more than 30 years ago and it was an extension to higher latitudes of ideas concerning the plasmasphere. *Axford* (1968), *Banks and Holzer* (1968, 1969), and *Marubashi* (1970) first studied quantitative estimates of ionospheric outflows using hydrodynamic transport equations to compute the expected character of polar wind outflows at high latitudes. There, low pressure is maintained by stretching of convecting flux tubes leading to an outflow. No solar wind influence in the polar cap and the lobe was used in the calculation. At that time, light ion flows of protons ($H^+$) and helium ions ($He^+$) were anticipated to be dominant ion species. The light ion outflows were confirmed by ionospheric observations of *Hoffman* (1970) and *Brinton et al.* (1971), while at the same time *Shelley et al.* (1972) discovered that a significant amount of oxygen plasma ($O^+$) was present in the magnetosphere during geomagnetically disturbed periods. These works promoted further investigations of the processes that influence the outflow transport of ionospheric plasmas, and their possible importance to the magnetospheric plasma content and dynamics. In fact, the initial focus was on the unpredicted abundance of oxygen outflow that was necessary to account for the magnetospheric observations.

Fig. 1.1 shows the Sun, the Earth's magnetosphere and the Sun-Earth interaction schematically. The region in the magnetosphere where we have investigated via outflowing $O^+$ 'probe' is also emphasized in the figure.

During this 30-year period, and perhaps in the future, we have pursued and are still pursuing the following questions to be answered through intensive modelling and observational investigations concerned with ionospheric outflows: What accelerates ionospheric ions to energies of 10s, 100s and 1000s of eV? How is the outflow of light and heavy ions distributed in space and time? Which outflow regions contribute to which magnetospheric regions? How much plasma does the ionosphere supply to the plasma sheet and ring current plasmas? How important is ionospheric plasma in the dynamics of the magnetosphere? Furthermore,

the global circulation or source-transport-loss process of terrestrial origin ions (mainly $O^+/N^+$) has been leaped into prominence when high-energy cold $O^+$ beams have been observed in the distant tail ($\sim$200 $R_E$) (e.g. *Seki et al.*, 1996). Additionally, there are several attempts of modelling that describe the transport of solar and ionospheric plasmas throughout the magnetosphere as functions of solar wind parameters (including the interplanetary magnetic field, IMF, conditions) and resultant changes in magnetospheric global plasma circulation (e.g. *Winglee*, 2000).

Importance is not limited on the Earth. Recently, thanks to many planetary explorations to unmagnetized/magnetized planets with/without atmosphere in the solar system, we have begun to pay more attention to investigations of Earth's magnetosphere-ionosphere-atmosphere dynamical structures in comparison to other situations on other planets. For example, if one detect any "$O^+$ outflow" from a planet, we can immediately conclude that (1) there is oxygen, in whatever chemical forms in the 'atmosphere' on the planet, (2) there are chemical process(es) converting oxygen into an ionized oxygen atom ($O^+$), i.e. existence of an 'ionosphere', and (3) there are physical processes that cause $O^+$ to escape. Therefore we can stress that the "$O^+$ outflow" investigations are 'cornerstones' in the planetary plasma physics.

In this thesis, I first introduce the background of ionospheric $O^+$ which at last gets energies more than keV at very high altitudes, because a keV-energy level is more than 100 times larger than Jean-escaping (thermal) energy level (10 eV). Therefore the ionospheric context in which $O^+$ is created is mentioned, and subsequently physical processes and mechanisms in which escaping $O^+$ get energized as the altitudes increase are mentioned (2.1 and 2.2 in Chapter 2). Secondarily, I look through the past observations of $O^+$ acceleration (including its energization and outflow process as well) in the polar region because this survey helps us to distinguish between what has been done and what is still unsolved (or unknown) (2.3 in Chapter 2), then the specific problems are pointed out at the end of this chapter (2.4 in Chapter 2). Thirdly, I outline the motivations and summarize on a series of my works, dividing my principal works into each section (Chapter 3). Finally, I mention about the future perspective related to my works (Chapter 4). Several appendices and four papers follow at the end.

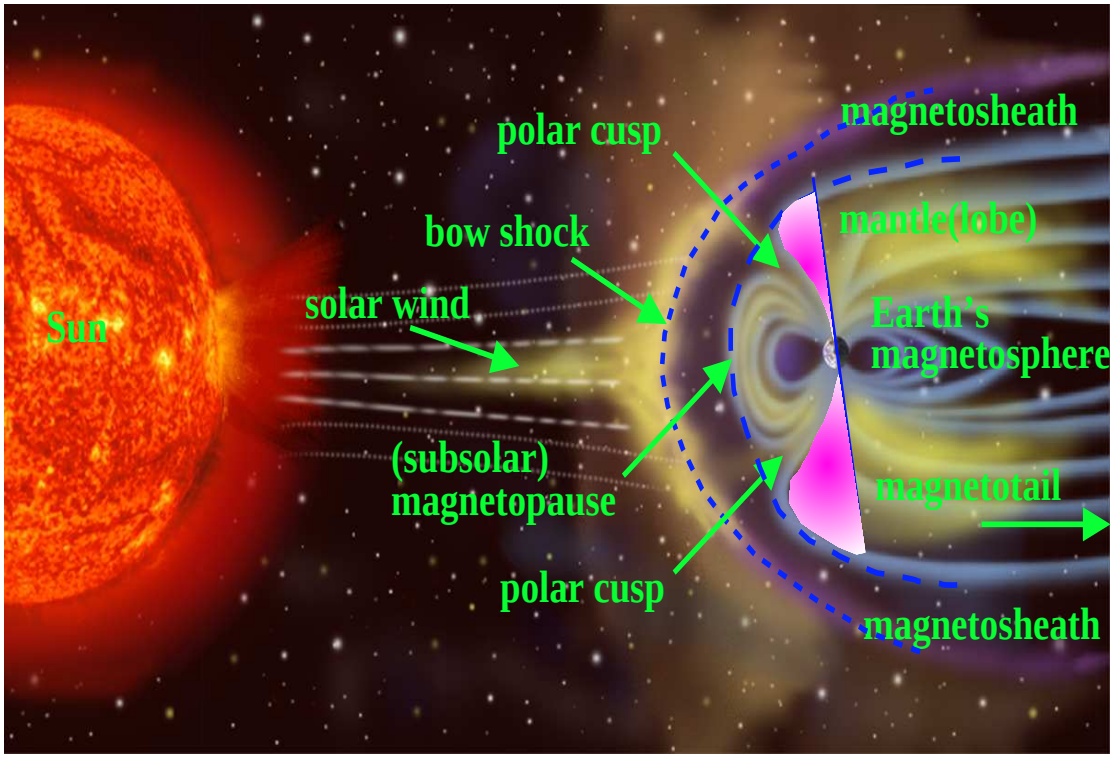


Figure 1.1: Schematic diagram of the Sun, Earth's magnetosphere and the Sun-Earth interaction. The region focused on in this thesis is emphasized. Several key terms and the corresponding locations are also displayed. Original picture from NASA (non-protected by copyright law unless noted).

# Chapter 2

# Background

The single-charged atomic oxygen ions ($O^+$) observed around the geosphere are undoubtedly of terrestrial origin. The solar wind-origin ionized oxygen is a hexa-charged particle ($O^{6+}$).

The single-charged atomic oxygen ions are created through photoionization process by solar EUV (extreme ultra violet) or soft X-ray. Major neutral species on the Earth ($N_2$ and $O_2$) are photoionized as follows

$$\begin{aligned} \mathrm{N_2} + h\nu &\rightarrow \mathrm{{N_2}^+ + e} \\ \mathrm{O_2} + h\nu &\rightarrow \mathrm{{O_2}^+ + e} \\ \mathrm{O} + h\nu &\rightarrow \mathrm{O^+ + e} \end{aligned} \tag{2.1}$$

The $O^+$ density profile peaks at the altitude of around 300 km for the daytime mid-latitude ionosphere (*Banks et al.*, 1976). The $O^+$ requires an energy gain of about 10 eV in order to overcome the gravitational barrier, however the temperature of the ionosphere is less than 10,000 K ($\sim$1 eV).

Therefore, the $O^+$ which have energies more than 1 keV can not in general gain such a huge amount of energy from thermal process in the ionosphere. To understand what we have done in our works, the origin of 'outflowing' $O^+$ is introduced in the context of the ionosphere and its structures, followed by escaping (and finally, upward flowing) $O^+$, then major physical processes in the magnetosphere, i.e. after leaving the ionosphere but not so far away from the Earth, e.g. up to 2–3 $R_\mathrm{E}$ altitudes.

## 2.1 Sources of ionospheric outflowing ions

### 2.1.1 The Ionosphere

On the Earth, upper atmosphere (above $\sim$80 km) which is called the *ionosphere* exists and continues up to about a few 1000 km altitude. The ionosphere has an altitude structure: The region with the maximum ionized particle density (up to $10^6$ particles/cm$^3$) at about 250–300 km is called the *F-layer*; Below the F-layer

there exists the *E-layer* (at ∼100 km) and the bottom of the ionosphere (∼80–100 km) there is the *D-layer*. The density profiles of heavier ion species ($O_2^+$, $N_2^+$, $NO^+$) peak around between the D-layer and the E-layer, The $O^+$ density peaks around the F-layer, and above the topside ionosphere the lighter ion species ($H^+$, $He^+$) become dominant.

**Thermospheric compositions**

The composition of ionospheric ions of the magnetospheric plasma source is fundamentally constrained by the composition and structure of the thermosphere which is the neutral atmosphere above ∼80 km altitude. The composition of the thermosphere is strongly dependent upon its temperature. Atmospheric hydrogen (H) is marginally bound by gravity at thermospheric temperatures, so a temperature increase produces significant escape of hydrogen atoms into space, increasing the H density in the geocorona above ∼2000 km altitude as well as decreasing the H density at lower altitudes. Thus the production of $H^+$ is reduced when thermospheric temperatures rise. The situation for helium atoms (He) is almost the same as that for hydrogen except for a lesser degree of temperature dependence. However, thermospheric heating has a completely opposite effect on the O density in the ionospheric altitude range. Oxygen atoms are strongly confined by gravity, so that a temperature increase during the solar maximum produces an increase in the scale height of O which leads to an order of magnitude higher density (than that during the solar minimum) of oxygen at ionospheric heights (*Cannata and Gombosi*, 1989).

**Diurnal and seasonal effects**

The ionospheric density varies diurnally due to the presence in the day and the absence in the night of the ionization (photoionization) of the neutral gas by the solar UV/EUV radiation. Typically the ion temperature is about 1000 K and vertically constant in the night, while it begins to increase at around 400 km altitude and is about 3000 K at around 1000 km in the day. There are also seasonal variations due to the inclination of Earth's spin axis.

**$H^+/O^+$ 'crossover' in the topside ionosphere**

The ion-neutral chemistry in the topside ionosphere is dominated by the reaction $H + O^+ \leftrightarrow H^+ + O$ (accidentally resonant charge exchange)(*Hultqvist et al.*, 1999) and this reaction tends to maintain the ions in approximately the same mixing ratio. The $H^+$ is favoured at altitudes where H is dominant, thus the elevated crossover level associated with thermospheric temperatures leads directly to reduced production of $H^+$ and increased content of $O^+$ in the upward flows through the ionosphere.

**Solar activity effect**

The solar cycle variation of UV flux influences the thermospheric temperatures and consequently the production of composition in the plasma outflow.

From the maximum to the minimum (or reversely) of a solar cycle, the variation of thermospheric temperature ranges from 500 to 2000 K which leads to a change in the O scale height as well as a change in the O density at F-layer peak heights. The ionosphere becomes a significantly better source of $O^+$ as the thermospheric temperature is raised. According to a modelling study by *Cannata and Gombosi* (1989), the increase of $O^+$ outflow flux from solar minimum to solar maximum was found to be over an order of magnitude.

### 2.1.2 Circulation at the topside ionosphere

Concerning possible sources of terrestrial (ionospheric) origin ions which are outflowing in the magnetosphere, primarily one is the polar wind generated from the high-latitude ionosphere consisting of lighter thermal ions ($H^+$ and $He^+$) and continually moving upward in the polar cap region, simultaneously convected toward the nightside plasma sheet boundary. Another is the upflowing ions originating from the dayside cusp/cleft region and the entire auroral oval in which parallel potential drops are in general associated with, and consequently, for dayside upflowing ions, dispersed over the polar cap toward also the nightside plasma sheet boundary by (anti-sunward) polar convections. Some of them, which are outflowing from the nightside auroral oval, are transported to the plasma sheet, then move to the inner magnetosphere by geomagnetic field gradient effect. On the other hand, the rest of them can be accessible to the plasma sheet if already on closed field lines after the reconnection, while others are lost through the magnetopause and mixed with the magnetosheath solar wind ions or travel to the long distance in the tail.

The ionospheric dynamics are different between at the low latitudes and at the high latitudes. Since $O^+$ outflow is the phenomenon at the high latitudes, we describe high-latitude ionospheric circulation.

**Convection**

The topology of horizontal (or convective) circulation streamlines at high latitudes changes abruptly from near-corotation to a double-celled convection pattern for a southward IMF ($B_z$<0) and a more complex convection pattern for a northward IMF ($B_z$>0). The typical features of this circulation pattern have been well summarized by *Heelis et al.* (1982) and *Heppner and Maynard* (1987).

**High latitude vertical flows – Polar wind**

The very low density, supersonic flux of cold light ions ($H^+$ and $He^+$) through the polar cap and into the magnetospheric lobes associated with high solar activity is called the *'classical' polar wind* (*Schunk*, 2000). This high latitude (i.e. at auroral and polar cap latitudes) vertical flow has been observed from at topside ionospheric heights up to 9 $R_E$ (*Brinton et al.*, 1971; *Hoffman and Dodson*, 1974, 1980; *Olsen et al.*, 1986; *Wu et al.*, 1992; *Abe et al.*, 1993a,b; *Yau et al.*, 1995; *Nagai et al.*, 1984; *Moore et al.*, 1997).

The flow in the polar cap is an ambipolar flow in which the ions are drifting faster than ambient electrons. Recent observations (e.g. *Su et al.*, 1998; *Moore et al.*, 1999) have shown that the polar wind is often variable in velocity and the variability is in some way related to polar rain electrons (hotter than ionospheric electrons) environment. The interaction of these two plasmas with large temperature differences can produce electric potential differences (*Hultqvist*, 1971).

The polar wind, a bulk ion flow in which all the ions acquire a bulk flow energy of up to a few eV in the direction parallel to the geomagnetic field, is observed at all local times poleward of the plasmapause (the outer boundary of the ionosphere). The significant components of polar wind are $H^+$, $He^+$ with some $O^+$ contributions. At a given altitude, the bulk velocities ($V_{H^+}$, $V_{He^+}$ and $V_{O^+}$) are ranked to $V_{H^+} > V_{He^+} > V_{O^+}$. For all species, the bulk velocity at a given altitude is higher on the dayside than on the nightside, due to the large ambipolar electric field in the presence of escaping atmospheric photoelectrons. The $O^+$ polar wind velocity starts to increase at an altitude of about 5000 km, reaches 1 km/s near 6000 km, and is $\sim$4 km/s near the Akebono apogee ($\sim$10,000 km) (*Abe et al.*, 1993a). The averaged velocity of polar wind is essentially independent of the magnetic activity level, however its variability is as large as 50% of the mean velocity at active times ($K_p$>4) and smaller at quiet times (*Abe et al.*, 1993a). Moreover, the polar wind velocity is correlated with the ambient electron temperature, thus it is believed that the acceleration of the polar wind ions is driven by the ambipolar electric field along the field line whose amplitude is dependent upon the electron temperature.

**Cleft ion fountain**

Many morningside and dayside ion outflow events are called *upwelling ions*, which are in principle gravitationally bounded, since the whole distribution has a net upward drift (*Lockwood et al.*, 1985a; *Moore et al.*, 1986; *Giles et al.*, 1994). Upwelling ions are usually observed in the morning sector of the auroral oval and the lower latitudes of the polar cap. The outflow is usually dominated by $O^+$, but all observed species ($H^+$, $He^+$, $O^+$, $O^{+2}$ and $N^+$) are energized to similar energies (*Hultqvist et al.*, 1999). Therefore, upwelling ions are distinguished from the 'classical' polar wind (i.e. cold supersonic flows composed of lighter ions, $H^+$ and $He^+$). Many upwelling ions are further (transversely) energized, becoming gradually more field-aligned (then may be labelled as *ion conics* at their initial stage), and can reach higher altitudes when drifting to higher invariant latitudes. Generally, upwelling ions fall down by gravitational bound unless additional heating. When upwelling ions are heated and flow upward due to the magnetic mirror folding, these ions are called *upflowing ions*.

Because of the low upward velocity compared to horizontal convection velocity, upwelling ions are spatially dispersed across the polar cap toward the nightside according to their time of flight.

### 2.1.3 Outflowing $O^+$ at mid-altitude (up to a few $R_E$)

$O^+$ outflows of energy up to a few keV have been observed over the auroral oval and polar cap region at altitudes 0.5–3 $R_E$ (*Shelley et al.*, 1976a; *Sharp et al.*, 1977; *Klumpar*, 1979; *Lockwood et al.*, 1985a; *Horwitz and Lockwood*, 1985; *Waite et al.*, 1986; *Abe et al.*, 1993a,b), and in the tail lobes (*Frank et al.*, 1977; *Sharp et al.*, 1981; *Candidi et al.*, 1988; *Hirahara et al.*, 1996b). The largest outflow fluxes are found near the dayside cleft region. Both amount and areas of $O^+$ outflows depend strongly on $K_p$ and solar wind dynamic pressure (*Norqvist et al.*, 1998; *Øieroset et al.*, 1999).

On the other hand, observations by means of the Akebono spacecraft have promoted the idea that steady $O^+$ outflow enhancements are originated from the polar cap region, or at least the sunlit part of the polar cap. The background theory for this idea is: sufficient photoelectrons liberating $O^+$ provid sufficient magnetospheric electron flux to develop an ambipolar electric drop for $O^+$ escapes.

**Ion beams and conics**

Ion beams are upflowing ions which have a peak flux along the upward magnetic field direction, and are generally observed above 5000 km (occasionally down to $\sim$2000 km). In contrast, ion conics have a peak flux at an apex angle (angle from the upward magnetic field direction), and are observed from $\sim$1000 km or below. Both ion beams and conics are commonly observed up to several earth radii (first observed by *Shelley et al.*, 1976a; *Sharp et al.*, 1977, and by satellites, e.g. S3-3 and Viking). They are dominated by $H^+$ and $O^+$ with energies ranging from 10 eV to a few keV. According to the statistical study of mid-altiude (up to $\sim$3 $R_E$) by *Yau et al.* (1984), the occurrence probability of ion beams ($>$1 keV) increases with altitude, while that of ion conics decreases with altitude. Concerning the evolution of distributions for both beams and conics, it is likely that most beams are due to acceleration by magnetic field-aligned electric fields (or parallel potential drops), however some may be due to the magnetic mirror folding of conics along the field lines. The apex angle of conics decreases with altitude more slowly than expected from adiabatic motion, i.e. conics might be continually heated as they move up the geomagnetic fields (*Miyake et al.*, 1996).

### 2.1.4 Effects of magnetic activity, solar cycle and seasons

The magnetic activity (as gauged by $K_p$ index) and solar activty (seasonal or solar-cycle variations of solar EUV radiation, measured as $F_{10.7}$ index) dependences of ion outflow processes have been reported, mostly on the outflow rates (see, e.g. *Yau and André*, 1997). According to these studies, the $K_p$ and $F_{10.7}$ dependences of outflow rates are clearer for $O^+$ than for $H^+$.

The influence of solar EUV radiation on $O^+$ outflow, appeared as seasonal and solar-cycle variations, can be understandable in terms of both ionospheric

and atmospheric scale heights. An enhanced solar EUV flux (in the summer and near solar maximum) will heat both the atmosphere and the ionosphere, and increase the scale heights. The presence of ions at a sufficiently high altitude, where the density is sufficiently low and the effects of collisions and charge-exchange are negligible, is important for ion outflow. As mentioned previously, the thermospheric/ionospheric heating lets neutral atomic hydrogen (H) escape, jumping over the gravitational barrier, resulting in a lack of source for $H^+$ outflow.

Recently, *Cully et al.* (2003) have reported both the solar wind parameters and the IMF hourly dependences of lower-energy ($<$70 eV) ionospheric outflows in terms of upward flow rates by means of the Akebono spacecraft observations (covered altitudes are between 6000–10,000 km). The upward flow rates of ionospheric ion outflows are well correlated to the solar wind dynamic pressure, the solar wind electric field and the variation of IMF in a hourly time-scale. A similar, but at higher altitudes (5.5–8.9 $R_{\mathsf{E}}$ geocentric) and under solar minimum period, result on correlations between solar wind parameters (including the IMF conditions) and the properties (density and parallel flux) of ionospheric ion outflows has been reported by *Elliott et al.* (2001). They also indicated that for higher $K_p$, thus higher convection over the polar cap region, most of observed $O^+$ are convected from dayside toward nightisde across the polar cap.

## 2.2 Physical processes

A large and variable amount of oxygen ions have been observed at plasma sheet energies during the high solar activity (*Shelley et al.*, 1972). This was not expected from the 'classical' polar wind theories and observations. Furthermore, the cold supersonic light ion outflows (i.e. 'classical' polar wind) are often accompanied by comparable fluxes of $O^+$, even under the conditions of low solar activity. These observations indicate that there is at least an additional acceleration (energization) process acting on $O^+$ in the magnetosphere.

There are many different physical processes that may accelerate ions to keV energy ranges in the magnetosphere. They include wave-particle interactions associated with different wave modes, parallel potential drops, centrifugal acceleration, discontinuity and shock, reconnection, and two-stream instability. These physical processes occur in different scales at different places in the magnetosphere. In the following subsections, only the processes which are closely related to my works are presented, therefore reconnection and shock (discontinuity) are not dealt with here.

### 2.2.1 Wave-particle interaction – Resonance and heating

Interaction of ions with electrostatic or electromagnetic waves can lead to energy transfer from the waves to the ions. The energization of ion conics is caused by the essentially perpendicular component of electric fields oscillating within some

frequency ranges. Several wave modes can cause perpendicular ion energization.

In the polar ionosphere, electromagnetic waves including Alfvén waves (large scale wave) are often observed.

**Heating by broadband low-frequency (BBLF) waves**

One common type of ion heating is associated with broadband low-frequency (BBLF) electric wave fields. These waves cover frequencies from less than one Hz up to several hundreds Hz, corresponding to the gyrofrequencies of major ion species at altitudes from $\sim$1000 km up to a few Earth radii ($H^+$ gyrofrequency [Hz]: $f_{c,H^+}$=1.5·10$^{-2}B$, $O^+$ gyrofrequency [Hz]: $f_{c,O^+}$=9.5·10$^{-4}B$, where $B$ is an intensity of magnetic field, ranging typically a few ten thousands nT to a few tens nT from the upper ionosphere up to the magnetopause). A maximum heating rate can be obtained under the assumptions that the perpendicular wave vector ($\boldsymbol{k}_\perp$) is much smaller than the inverse of the ion gyroradius ($1/r_c$), and that the left-hand polarized fraction of the waves is heating the ions. A significant fraction of the BBLF emissions may be ion acoustic waves (*Wahlund et al.*, 1996) or electrostatic ion cyclotron (EIC) waves (*Bonnell et al.*, 1996).

The observed ion distribution functions give us some information concerning the wave modes, and sometimes all ions seem to be energized by the waves (bulk heating) forming an essentially Maxwellian distribution. The broadband waves together with elevated conics (the peak flux has an oblique angle against the direction of magnetic field, at the same time obtaining parallel velocity due to divergence of the magnetic field) have been observed in the central plasma sheet (*Chang et al.*, 1986). The broadband emissions together with low-energy elevated conics and bulk heated ion conics have been observed in the morningside and dayside magnetosphere (*Moore et al.*, 1986; *Norqvist et al.*, 1996). These observations indicate that broadband waves sometimes may heat the entire ion population, however there is no statistical study on ion distributions during various conditions. Furthermore, waves classified as broadband emissions may have a composition that generates a high energy tail of the ion distribution (e.g. caused by low hybrid waves, $f_{LH}$ for corresponding frequencies), as opposed to bulk heating. It should be noted that the morning side and dayside magnetosphere seem to be the most important source of ionospheric ion outflow whose distributions show clear signs of bulk heating.

Gradual stochastic heating, i.e. perpendicular resonant ion energization by waves, e.g. the ion gyrofrequencies, together with upward motion in a diverging geomagnetic field (i.e. mirror folding effect) can explain many of the observed elevated conics (*Temerin*, 1986; *Peterson et al.*, 1992; *Miyake et al.*, 1996). However, some elevated conics may have been accelerated upward by a parallel electric field (*Klumpar et al.*, 1984) rather than this parallel energization associated with perpendicular ion heating. The parallel energization (or accleration) is mentioned in the next section.

**Magnetic moment pumping (Ponderomotive force)**

Sometimes broadband spectra correspond to large amplitude electric field fluctuations (several hundreds mV/m). These fluctuations occur primarily at low frequencies with a power spectral density maximum below 1 Hz. Such fluctuations have been observed together with ion conics with average energies of a few keV (occasionally up to tens of keV) at altitudes of about 10,000 km by the Viking satellite (*Hultqvist et al.*, 1988; *Block and Fälthammar*, 1990). *Lundin and Hultqvist* (1989) proposed a simple mechanism for the energization of ionospheric ions, denoted "magnetic moment pumping", where the magnetic moment of ions is gradually increased by electric field variations.

The simultaneous observation of strong low-frequency electric field fluctuations and ion energization (e.g. *Lundin and Hultqvist*, 1989; *Lundin et al.*, 1990) can be interpreted as the result of field-aligned ponderomotive forcing by Alfvén waves (*Guglielmi and Lundin*, 2001). Ponderomotive forcing implies the transfer of wave energy and momentum to particles. A traveling wave may transfer energy and momentum in the direction of wave propagation (gradient/Miller force). An interesting property of ponderomotive forces is that they may be effective also well outside the wave resonance regime. The ponderomotive magnetic moment pumping force is unique in that it always points in the direction of decreasing (diverging) magnetic field, regardless of the wave propagation direction (*Guglielmi and Lundin*, 2001). This implies that waves propagating downward in the Earth's dipole field can cause upward acceleration of ionospheric plasma.

### 2.2.2 Parallel energization

There are three major processes for parallel energizations. One is the parallel potential drops, another is the centrifugal acceleration, and a third is the mirror folding effect converting the perpendicular energy to the parallel energy. Ponderomotive force (mentioned in the previous section, *Wave-particle interaction*) also contributes to a parallel particle acceleration. Therefore, in addition to the former three processes, more description on ponderomotive force is added in this section.

**Parallel potential drops**

The theory of field-aligned/parallel potential drops above aurora originates from *Alfvén* (1958). The first observational evidence for parallel acceleration processes came from rocket measurements of precipitating electrons in the auroral region (*McIlwain*, 1960; *Evans*, 1968). The electron energy distributions show a peak at several keV, and are shown to be consistent with acceleration of the electrons through an electric potential drop parallel to $\boldsymbol{B}$.

The observation of upward field-aligned ion beams at altitudes above $\sim$5000 km in the auroral region also shows evidence of such parallel electric fields (*Shelley et al.*, 1976a; *Gorney et al.*, 1981). The observations done by the Viking satellite show an altitude distribution of field-aligned electric field. *Marklund*

(1993) has reported that the average parallel electric fields measured by the Viking double-probe experiment are directed upward for altitudes above 6000 km and downward below 4000 km. This measurement is consistent with other observations from Viking. *Mälkki and Lundin* (1994) found that the dayside parallel acceleration region lies within the altitude range 4000–12,000 km.

**Centrifugal acceleration**

One way in which convection can affect outflows is through centrifugal acceleration. *Cladis* (1986) first proposed the centrifugal force in the reference frame of the plasma convecting across the polar cap as an important contributor to the acceleration of $O^+$. *Horwitz et al.* (1994a) suggested that this acceleration process is sufficient for the significant enhancement of $O^+$ escape outflows. However, *Demars et al.* (1996) argued that the centrifugal force is only effective above a few $R_E$. They cite observations showing heated features of escaping $O^+$ at lower altitudes. If the centrifugal force is a significant contributor, it increases the parallel velocity of the $O^+$ outflow relative to the transverse or convective flow. Therefore, it is likely that heating effects are dominant in enhancing the number flux of escaping $O^+$ at lower altitudes, i.e. below a few $R_E$.

**Parallel ion heating**

The diverging magnetic field geometry leads to a folding effect (via magnetic mirror force) for upgoing ions, i.e. transverse energy is converted to parallel energy with increasing altitude. In this mirror folding process, transverse ion heating contributes in some way to the parallel ion temperature, results in a substantial thermal spread in the parallel ion beam distribution. Parallel heating seems to be a general feature of the parallel acceleration region, being roughly proportional to the 'electrostatic' field-aligned acceleration. However, *Lundin and Eliasson* (1991) have shown that a heated feature can be seen in the parallel ion beams, which is of the order of several tens of percent of the average beam energy, and ion beams have a higher perpendicular temperature than parallel temperature as a general trend.

*Bergmann and Lotko* (1986) have discussed that faster $H^+$ coexisting with slower $O^+$ (as a minority species) within ion beam regions can support parallel heating through a two-stream interaction. The $H^+$ distributions are asymmetrically heated in the parallel direction, with the high velocity side of the distribution remaining 'cold'. Such a distribution of $H^+$ indicates that energy from the positive $df/dv$ (differentiation of the distribution function $f$) part of the $H^+$ distribution is transferred to and heat the $O^+$ distribution.

**Ponderomotive force acceleration**

As previously mentioned, traveling waves may create ponderomotive forcing, i.e. a transfer of energy and momentum to particles, causing particle acceleration. For instance, kinetic Alfvén waves propagating along magnetic field lines are candidates for parallel particle acceleration. Theoretical analysis shows that

ponderomotive magnetic moment pumping in the Earth's magnetic dipole field provides an upward field-aligned force by Alfvén waves regardless of wave propagation direction (*Guglielmi and Lundin*, 2001). This means that wave propagating down to the ionosphere may lead to upward parallel acceleration of ionospheric plasma.

## 2.3 Past observations related to $O^+$ acceleration in the polar region

In this section, past observations are reviewed and summarized concerning ionospheric ion outflows and accelerations in and/or in vicinity of the polar cap region. As mentioned in Chapter 1 (Introduction), the studies of ionospheric outflows have been continued for more than 30 years. Since the mid-70's, many satellites have been launched and involved in *in situ* observations of ion outflows above the upper ionosphere in the polar cap region, either with higher-energy coverage or with higher-altitude survey, or with both.

We first mention the Russian Prognoz-7 satellite observations (inclination about 65°, apogee 32 $R_{\mathsf{E}}$). This satellite's orbits provided the measurements of the high latitude magnetopause, magnetosheath, and bow shock. *Lundin et al.* (1982) have showed that ionospheric origin beams observed in the regions connected to the dayside flank boundary layer and plasma mantle have much broader energy bands than expected from adiabatic particle motion, suggesting the presence of pitch angle scattering or transverse acceleration processes at such high altitudes above 4.7 $R_{\mathsf{E}}$. *Eklund et al.* (1997) have reported two types of $O^+$ populations in the high latitude magnetosheath on the basis of the Prognoz-7 observations. They found that the first type seen in both the 1.17 keV and the 3.8 keV channel of the detector can be explained by acceleration at the high latitude magnetopause, e.g. a rotational discontinuity. The second type (seen only in the 1.17 keV channel) showed a correlation between $O^+$ in the magnetosheath and positive IMF $B_z$ or low geomagnetic activity (i.e. indicated by low $K_p$). This indicates a direct escape through the magnetopause during low convection fields. We learn from this observation that a significant loss of $O^+$ to the interplanetary medium may occur when we otherwise expect it to be small.

Regarding observations by Dynamics Explorer-1 (DE-1), *Horwitz et al.* (1992) have introduced the presence of two ion populations in the polar cap: One is high-speed (10–30 eV or higher) polar beams observed on or near the field lines of auroral arcs, while the other is low-speed (generally less than 10 eV) streams observed on or near field lines threading the polar cap. Additionally, *Giles et al.* (1994) have reported that low-speed streams were cleft ion fountain origin, poleward dispersed by high-latitude convection electric field, while high-speed polar beams experienced additional acceleration in which ion energy becomes greater than 50–60 eV at late afternoon local time sector.

Next we mention the Swedish Viking satellite observations. *Eliasson et al.*

(1987) have reported that acceleration of narrow beams of upflowing ions below the spacecraft altitude (up to 13,500 km =$\sim$2 $R_E$) by field-aligned potentials are typically observed. *Lindqvist and Marklund* (1990) have reported the distribution of small-scale electric fields and the presence of parallel (to the geomagnetic field) electric fields up to about 11,000 km (=1.7 $R_E$) altitude. The electric fields are directed in general upward with an average value of 1 mV/m, but depended on altitude and plasma density.

Ionospheric outflows at two different altitudes (5000 km and 8 $R_E$) observed by the Polar satellite (*Su et al.*, 1998) exhibited that at 5000 km, $H^+$ is supersonic upflow, while $O^+$ is subsonic downflow and cleft ion fountain origin is due to density decline from dayside to nightside, and at 8 $R_E$ both $H^+$ and $O^+$ are supersonic outflows. They also suggested the existence of an electric potential layer near and/or below 8 $R_E$ due to the typical bulk ion field-aligned velocities ratio of $V_{O^+}$:$V_{He^+}$:$V_{H^+}$$\sim$2:3:5.

With respect to ion outflows and/or accelerations in the auroral zone, the Fast Auroral SnapshoT (FAST) observations should be mentioned. On 24 and 25 of September, 1998, the Polar spacecraft observed intense outflows of terrestrial ions in association with the passage of an interplanetary shock and coronal mass ejection (CME). The orbit of the FAST explorer was in the noon-midnight meridian during this ion outflow event, and passed through the dayside cusp region at $\sim$4000 km altitude every 2.2 hours. FAST was therefore able to monitor the ion outflows subsequently observed by Polar (*Strangeway et al.*, 2000). Subsequently, it is mentioned in the same work above that as a consequence of the reconnection of cusp-region field lines at the magnetopause, the flux transport resulted in electromagnetic energy being transmitted along the field lines to the ionosphere as Poynting flux. This Poynting flux was presumably caused by the strong IMF $B_y$ ($\sim$40 nT), and the dominant energy input to the cusp-region ionosphere. *Strangeway et al.* (2000) continued to conclude that the energy carried by downward directed Poynting flux is dissipated as heat within the ionosphere, through Joule dissipation, and the heating will tend to increase the ionospheric scale height, allowing ionospheric ions to gain access to the altitudes where transverse ion heating via ELF wave can occur. The most intense precipitating electron energy flux and ion outflows were found in the polar cap boundary region during magnetospheric substorms by the measurement of FAST spacecraft (*Carlson et al.*, 2001). This boundary region begins at the open magnetic field boundary identified by polar rain electrons, and bursty, magnetic field-aligned electron fluxes are associated with intense Alfvén waves rather than with quasi-DC potential structures. Intense low frequency waves generated by the electron bursts produce intense ion heating. Ion conic outflows were enhanced exceeding $10^9$ $cm^{-2}s^{-1}$ compared to typical values of $10^8$ $cm^{-2}s^{-1}$ during successive substorms associated with magnetic storms with enhanced $O^+$ composition. *Su et al.* (2002) identified low frequency waves as propagating Alfvén waves with frequencies of 0.2–1 Hz, and *Tung et al.* (2002) have reported that the discrepancy, in which polar cap boundary ion conics consisted primarily of oxygen ions,

while protons and helium ions were predominant in earlier studies, cannot be explained either by the solar cycle or seasonal variation.

There are several Cluster observations concerning ion acceleration associated with the polar cap region. *Sauvaud et al.* (2003) and *Fontaine et al.* (2004) have recently reported acceleration structures above the polar cap at relatively high altitudes (5–6 $R_E$). They mentioned that these structures involve outflowing ion beams, downgoing electrons, and convergent electric fields. Many cases of low energy outflowing ion beams indicated that parallel electric field is not strong enough to cause the loss of the precipitating electrons.

To mention one more finding relevant to my thesis' works: The Geotail observation found $O^+$ existing in the long-distance tail region (up to a few hundreds $R_E$). According to *Seki et al.* (1998a,b), cold $O^+$ beams (COBs) (some of them have energies ranging $\sim$3–10 keV) in the lobe/mantle show the necessity of an extra energization of $\sim$2.7 keV on average to the polar $O^+$ outflows so as to supply COBs in the distant tail. However, there were not many observations surveying the dayside high-altitude (principally above 5 $R_E$ altitude) polar region before the Cluster project, thus it was difficult to verify the above suggestion in terms of either case studies or statistical studies. Unprecedented successful observations done by the Cluster spacecraft lead us to survey this "not well-known" region in terms of energization (heating and acceleration) process(es) of terrestrial origin ion outflows, and chance to broaden our knowledge on the issue.

## 2.4 Specific problems

In principle, the terrestrial origin $O^+$ can be seen everywhere in the magnetosphere, even in the magnetosheath or in the long-distance tail region. However, the circulation of $O^+$ in the magnetosphere, or the loss rate of $O^+$ in the magnetosheath or the long-distance magnetotail are still unanswered to date. Furthermore, it has been well established that there are many physical processes in which $O^+$ can be accelerated and/or energized "in the mid-altitude region". This means that we lack of one piece of the puzzle, i.e. an identification of energization and/or acceleration processes in the high-altitude (inside the magnetopause) region. My works on this thesis were motivated from such a situation. Additionally, the region we have focused on (see Fig. 1.1) is the dayside high-altitude region of the magnetosphere, i.e. from the poleward cusp toward the polar cap via the plasma mantle along the open geomagnetic field lines and very close to the magnetopause. This means that one can examine direct/transition effects of the solar winds and/or the IMF which are an energy source as well as a driver of the magnetospheric dynamic processes. There have been many studies on the correlation between $O^+$ outflows and the solar activity at relatively lower altitudes, however there is no study on either an altitudinal dependence or a correlation between the energy of outflowing $O^+$ and the solar activity. Therefore, this became also one of the motivations for this thesis' works.

# Chapter 3

# Summary of thesis' works

In this chapter and hereafter, one specific region will be focused on in terms of ionospheric ion outflows and their energization/acceleration mechanisms. The specific region to be focused on is "dayside high-altitude and high-latitude (or polar) region", more precisely, the region between 6–12 $R_{\mathsf{E}}$ geocentric distance (or 5–11 $R_{\mathsf{E}}$ in altitude) and between 75–90 degrees in invariant latitude (ILAT) in the dayside sector. This region is located poleward dayside cusp (or auroral oval), topographically continued to plasma mantle and polar cap toward the magnetic pole, and upper-most of this region is very close to the magnetopause boundary theoretically. Actually, this region has not been surveyed systematically (or statistically) in previous satellite observations, therefore people infer what happens in this region just by analogy from low-/mid-altitude observations. However, this region has specific features: embedded in relatively weaker divergent geomagnetic fields and in contact more directly to the solar winds via the magnetosheath. Observing the dayside high-altitude region of the magnetosphere (the exterior cusp toward the polar cap, via the mantle) enables us to examine direct/transition effects of the solar wind and/or the IMF as an energy source for or a driver of the magnetospheric dynamic processes.

Recently, *Nilsson et al.* (2004) (and Paper IV) have reported that field-aligned upgoing $O^+$, observed above 4 $R_{\mathsf{E}}$ in altitude near the poleward cusp and/or the mantle region, show a heated signature in the velocity distribution. This means that there is a heating process at higher altitudes than we expected. Furthermore, they also reported that field-aligned upgoing $O^+$ show isotropic velocity distributions, i.e. neither 'conics' nor 'beams' but hot in spite of taking mirror folding effect into account, and that on a few occasions outflowing $O^+$ form a shell-like distribution at the highest altitudes (i.e. altitudes above 7 $R_{\mathsf{E}}$). There were many observations and studies on ion beams and conics observed mostly at the mid-altitudes (up to $\sim$3 $R_{\mathsf{E}}$), but there has been few or almost no systematic observations in the dayside high-altitude magnetospheric region in terms of dynamics (physical processes) of farther upflowing (or outflowing) ionospheric ions. In the following sections, unknown or unsolved issues/problems related to the dayside high-altitude outflowing ionospheric ions will be mentioned, through a case

study (Paper I) and a statistical study (Paper II). Paper III is actually an extended work of Paper II, dealing with relationships between the properties of dayside high-altitude polar outflowing $O^+$ and the solar wind parameters/the IMF conditions. However, with Paper III included, the solar wind energy/momentum transfer into the magnetosphere can also be discussed. Paper IV is cited as the occasion demands in this whole section.

## 3.1 Distribution functions of dayside high-altitude (above 5 $R_E$) outflowing $O^+$

### 3.1.1 Overview

The energized part of the ionospheric-origin ion outflow is associated with the auroral oval and is observed as beams and conics at mid-altitudes (up to $\sim$3 $R_E$) (*Yau and André*, 1997, and references therein). A beam has a peak flux centred along the geomagnetic field line, while the differential flux peaks at an oblique angle off the field-aligned direction for conics. Concerning the location of observing beams and conics, conics dominate the ion outflow in the cusp region, while beams are the main contributor to the ion outflow pre-noon and post-noon outside the cusp region (*Øieroset et al.*, 1999). The dayside upflowing ions, originated from the low-altitude cusp/cleft region, are first perpendicularly heated in the cusp region (the formation of conics), then accelerated by the magnetic mirror folding. Therefore, conics are seen at low altitudes, and as the altitude increases conics become less dominant (or evoluted to 'bimodal' or 'elevated' conics) and beams are observed more frequently.

*Lundin et al.* (1995) have reported that a good correlation between ion beam energy and the solar wind velocity by means of the observation of Viking spacecraft at middle altitudes ($\sim$3 $R_E$) in the near 14 MLT. To explain this solar wind-magnetospheric interaction via the ionospheric field-aligned upgoing ions, they have suggested a similar process of ions "picked-up" in the solar wind. The "picked-up" $O^+$, that have been studied well in the solar wind-comet interactions or recently in the solar wind-Martian escaping oxygen atoms interactions (e.g. *Cravens et al.*, 2002), are created by the neutrals and almost at rest in the solar wind frame of reference. The new-born ionized particles are initially accelerated by the solar wind convective electric field and partially picked up by the solar wind. It is also known that, from cometary studies, picked-up ions follow cycloidal trajectories, therefore a ring (or toroidal) distribution is formed in velocity space with a drift velocity parallel to the magnetic field initially in the absence of waves. However, this ring distribution is unstable and generates Alfvén waves via an ion cyclotron instability, which then can modify the distribution by pitch angle scattering into nearly isotropic in the solar wind reference.

Regarding 'ring' or 'shell-like' distributions observed "closed to the Earth" (except the bow shock region), for example, *Roth and Hudson* (1985) have

demonstrated that ring distributions of magnetosheath ion injections, which have been observed by both S3-3 and Dynamics Explorer-1 (DE-1) at $\sim$1–4 $R_E$, can generate lower hybrid (LH) waves by means of kinetic simulations. *Fuselier et al.* (1988) have reported solar wind $He^{++}$ and $O^{6+}$ shell-like distributions in the magnetosheath. Both $He^{++}$ and $O^{6+}$ distributions are centred on the downstream $H^+$ bulk velocity and they have suggested that the formation of shell-like distributions might occur through a coherent wave-particle interaction and/or by scattering in the existing magnetic turbulence in the sheath. Recently, *Sundkvist eq al.* (2005) have reported waves with frequencies near the proton gyrofrequency in the high-altitude cusp, which can be generated by the precipitating ions (protons) that shows shell-like distributions. However, above these are all solar wind-origin ions' features.

The latest companion study by *Hobara et al.* (2005) has dealt with the EFW (Electric Field and Wave experiment) data for examining high-altitude and high-latitude wave activities from one of the same events presented in Paper I, and they preliminarily reported that there are waves with frequencies near $O^+$ gyrofrequency ($<$1 Hz) and the BBLFs (above 10 Hz).

A shell-like configuration indicates a pitch angle scattering or at least ion isotropization process via wave-particle resonant interaction. Concerning the wave mode related to the observation in which a shell-like distribution has been seen, we can not exclude a wave generation by a two-stream instability under the condition that flows of both $O^+$ and $H^+$ coexist. Since the same bulk velocities of upward going $H^+$ and $O^+$ (*Nilsson et al.*, 2004, and Paper IV) are a result of two-stream instability.

### 3.1.2 Summary of Paper I

In Paper I, a shell-like distribution in "terrestrial origin" $O^+$ velocity space, observed above the altitudes of 7 $R_E$ (up to $\sim$11 $R_E$) by means of the CIS (Cluster Ion Spectrometry experiment) instrument onboard the Cluster satellite, is presented. This shell-like distribution consists of the lower energy (cold) populations centred along the field line (except perpendicularly sifted by the convection drift) and the higher energy as well as almost mono-energetic population building up (mostly a partial) half-spherical configuration. In contrast to the previous works mentioned above, this shell-like distribution in $O^+$ velocity space was observed inside/closed to the magnetopause altitudinally and in and/or near the poleward cusp/the mantle latitudinally. This paper has reported a couple of cases on shell-like distributions in $O^+$ velocity space. What the physical process causeing a shell-like distribution 'inside' the magnetopause, is still waiting to be investigated in the future.

According to the geomagentic field data provided by the FGM (FluxGate Magnetometer) instrument, two events were observed close to the magnetopause, others were observed in the poleward cusp or the mantle region. All the cases

were observed above 8.5 up to 10 $R_E$ geocentric distance. The altitude interval indicates clearly the region where we suggest additional energization/acceleration mechanism(s) for dayside outflowing $O^+$.

The first event is observed near the poleward cusp or in the mantle regions. Both $H^+$ and $O^+$ display half-spherical or partial shell-like velocity distributions. These features are clearly seen when one looks at distribution functions ($f(v)$): Field-aligned upward-going populations of $O^+$, $f(V_\parallel)_{O^+}$, displays partially overlapped two distributions, while perpendicular populations, $f(V_\perp)_{O^+}$, have one clear distribution which matches the distribution of higher velocity (or energy) of $f(V_\parallel)_{O^+}$. On the other hand, both field-aligned upward-going and perpendicular populations ($f(V_\parallel)_{H^+}$ and $f(V_\perp)_{H^+}$) of $H^+$ ions are almost the same, except for higher velocity (or energy) skirt seen in $f(V_\perp)_{H^+}$.

Second and third events are observed in the cusp region and very close to the magnetopause. The features remarkably seen in these events are; $O^+$ velocity distributions are no longer partial shell-like, but highly heated and forming a half-sphere. Note that this half-sphere distribution might be determined by upper limit energy detection ($\sim$38 keV) of the instrument, and in Paper I, instead of "half-sphere", a "dome-shape(d)" is used. However, the peak flux in the half-sphere velocity distribution is centred along the field-aligned direction, therefore it is not a typical conic-formation. On the other hand, the velocity distribution of field-aligned upward-going $H^+$ ions in the same region displays sometimes a 'pan-cake' or a 'conic-like' formation.

## 3.2 Energization and/or acceleration of dayside high-altitude outflowing $O^+$

### 3.2.1 Overview

The work presented in Paper II was motivated by and done from three perspectives: There have been many statistical studies to date on ionospheric outflowing ions (originated from both dayside upflowing ions and polar wind) from the upper ionosphere height to the apogee of the Polar satellite ($\sim$9 $R_E$ geocentric distance) under different seasonal and/or solar cycle conditions (e.g. *Elliott et al.*, 2001; *Cully et al.*, 2003), however very few surveys in the dayside high-altitude (i.e. above 5 $R_E$ in altitude) polar region under the descending phase from the latest solar maximum (from 2001$\sim$) (e.g. *Lennartsson et al.*, 2004). To survey high-energy (e.g. more than 1 keV) outflowing $O^+$ systematically for the purpose of confirming that there are persistent $O^+$ outflows with higher energies in the dayside high-altitude and high-latitude polar region (e.g. *Eklund et al.*, 1997; *Seki et al.*, 1998b). How do field-aligned upgoing $O^+$ behave in response to a geomagnetic activity (in this case, measured by $K_p$ index)? Instead of investigating the ordinary properties (e.g. moments), we have focused on the energy (symbolized as $PE$ in Paper II) of field-aligned upgoing $O^+$ populations which

have a maximum differential particle flux (same as $MDPF$ in Paper II).

On the other hand, the flux of ionospheric outflow is affected by the solar conditions, i.e. it increases as solar EUV flux ($F_{10.7}$) increases (*Yau and André*, 1997). *Norqvist et al.* (1998) also showed that $O^+$ ion outflows are strongly $K_p$ dependent. Recently, *Cully et al.* (2003) have reported correlations between the $O^+$ ion outflow rate (energy range from $<$1 to 70 eV, and observed by means of the Akebono satellite) and the solar radio flux ($F_{10.7}$), geomagnetic activity ($K_p$) and the solar wind parameters. Similar to the previous works, we have investigated the $K_p$ dependence on $O^+$ ion outflows in the high-altitude and high-latitude region.

The outflowing $O^+$ are persistently observed in the dayside high-altitude and high-latitude region by the Cluster spacecraft. The data set provided by the Cluster CIS/CODIF instrument, sampled during year of 2001–2003 from January to May, has been utilized to examine the properties of outflowing $O^+$. Regarding the properties of outflowing $O^+$, chiefly observed in the dayside high-altitude and high-latitude region, we have focused on looking at the energy of maximum (or 'dominant') differential particle flux, abbreviated to $PE$, and the maximum differential particle flux, $MDPF$, because the typical time-energy spectrogram of corresponding $O^+$ displays a very narrow (sometimes almost mono-energetic) energy band, both spatio and temporal long-lasting followed by the spacecraft traversals (See Fig. 3.1). Therefore both $PE$ and $MDPF$ are good variables for our investigations The plots of both $PE$ and $MDPF$ are shown as functions of geocentric distances ($R_\mathsf{E}$) and invariant latitudes (ILAT) in the bottom panel of Fig. 3.1, using the same data set shown in the upper panel of Fig. 3.1.

### 3.2.2 Summary of Paper II

First of all, we confirmed that outflowing $O^+$ with more than 1 keV are commonly observed above 10 $R_\mathsf{E}$ geocentric distance and above 85 deg ILAT in the dayside location. This disproved a conventional view that polar outflowing $O^+$ consisted of cusp/cleft origin usually have the energy less than 1 keV.

Second, the latitudinal distribution of outflowing $O^+$ at 6–8 $R_\mathsf{E}$ geocentric distance is consistent with velocity filter dispersion from a source equatorward and below the spacecraft, e.g. from the cusp/cleft region. However, at 8–12 $R_\mathsf{E}$ geocentric distance the latitudinal distribution of outflowing $O^+$ cannot be explained by velocity filter effect only, even though we assume one of the strongest magnetospheric convection cases based on the observation. These results suggest immediately that additional energization or acceleration process for outflowing $O^+$ occurs in the dayside high-altitude and high-latitude region (See Fig. 3.2 and Fig 3.3 in the end of this section).

Subsequently, we examined possible candidates for that (those) energization and/or acceleration mechanism(s). The main energization/acceleration mechanisms that have been known for ionospheric $O^+$ from the low-/mid-altitude observations are wave-particle interaction (resonance and heating), field-aligned

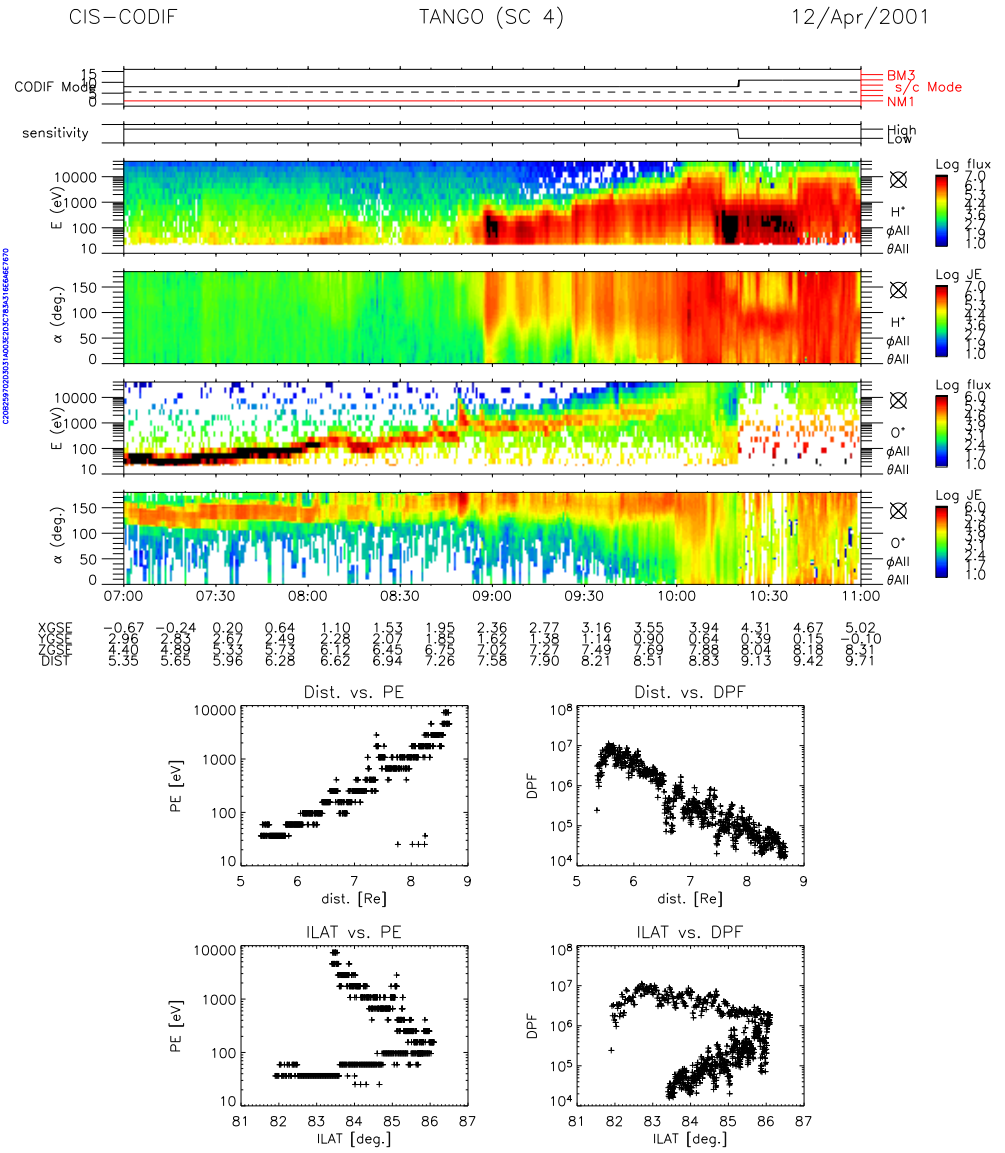


Figure 3.1: (**Upper**) A sample data provided by the Cluster CIS/CODIF instrument. The 5th and 6th panels, from the top, show time-energy spectrogram and time-pitch angle distributions of $O^+$. As seen in the panels, field-aligned upgoing $O^+$ with narrow energy band were observed continually in long time period, i.e. from 07:00 UT to 10:00 UT. (**Bottom**) The $PE$ and $MDPF$ distributions as functions of geocentric distance and ILAT are also shown. The data set is the same as the above.

'electrostatic' potential drops, and centrifugal acceleration. At low altitudes, *Norqvist et al.* (1998) have reported in their statistical study that most $O^+$ heating and outflows were caused by ion energization associated with BBLF waves and that the major source of $O^+$ ion energization is located in the pre-noon auroral region based on the Freja satellite observations (between 50° to 75° corrected geomagnetic latitudes, CGL, and altitudes 1400–1750 km). Field-aligned

(or simply, 'parallel') 'electrostatic' potential drop is another obvious acceleration mechanism which is confirmed by mid-altitude satellite observations (e.g. *Lundin et al.*, 1995; *Eliasson et al.*, 1996). The increase of $O^+$ outflow velocity below 5 $R_E$ can be explained in part by the centrifugal acceleration (*Ho et al.*, 1994). Concerning the centrifugal acceleration, refer to *Cladis* (1986) and *Horwitz et al.* (1994a). However, it is not clear yet whether heating by waves and acceleration by parallel potential drop confirmed at low-/mid-altitudes are sufficient for keV $O^+$ in the high-altitude region.

The centrifugal force can partially explain the energy gain, however there is a serious discrepancy between the supposition and the observation. If outflowing $O^+$ are accelerated only by centrifugal force, the distribution in velocity phase space is expected to display a "cold beam", however, the observed velocity distributions showed a 'heated' signature. The observation indicated obviously that outflowing $O^+$ were 'energized', i.e. heated and accelerated.

Another possible mechanism is ponderomotive force where waves and particles interact non-resonantly in the presence of very low frequency and large amplitude electric fields. By a very simple way of estimating the energy gain, ponderomotive force can also partially explain the energization of outflowing $O^+$. However, there are many assumptions for energy gain estimation, thus we need more data for more certain conclusions.

There is another acceleration mechanism by analogy from the mid-altitude observations: Parallel potential drops. However, parallel potential drops are usually too weak to accelerate ions to keV level at mid-altitudes in the dayside cusp/polar cap. Additionally, there is no systematic observation detecting high-altitude electrostatic kV potential drops, and furthermore, our one case study showed that field-aligned upgoing velocities of both $H^+$ and $O^+$ ions are almost the same, thus explaining the observation in terms of acceleration by parallel potential drops we might take two-stream instability into account as well.

Finally, we found a tendency to observe keV $O^+$ ions at high altitudes is more obvious for $K_p \geq 5$ than $K_p \leq 3$. We do not know if this $K_p$ dependence is due to the velocity filter effect (caused by magnetospheric convection) or due to an unknown energization mechanism. Therefore, we further investigated the properties of outflowing $O^+$ in response to other geomagnetic activities, e.g. measured by 1-minute $ASY/SYM$ indices. Moreover, a study should be made of both the solar wind parameters and the IMF conditions because high $K_p$ index is closely related to strong magnetospheric convection which is in general caused by solar wind influence. This issue is dealt in the next paper (Paper III) in detail.

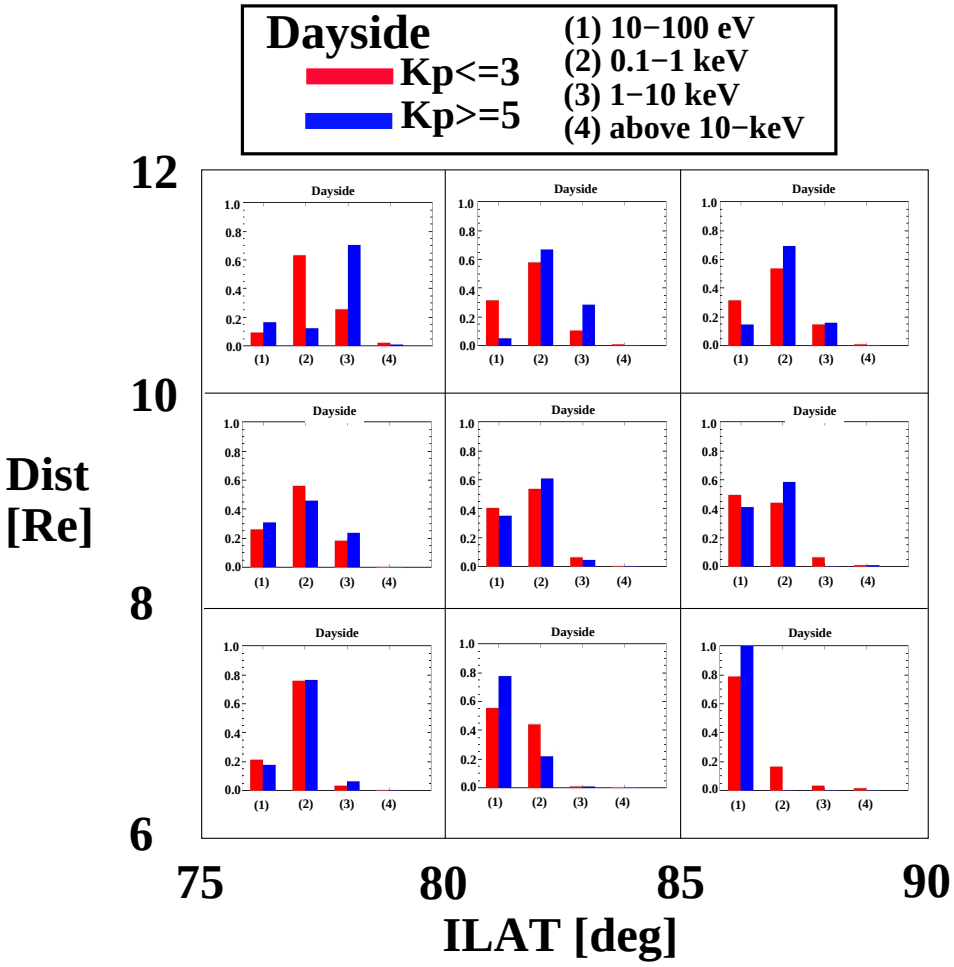


Figure 3.2: The occurrence rates of different $PE$ levels in the dayside high-altitude and high-latitude region. The whole region is divided into $2R_E \times 5^\circ$ subregions, and the pairs of bars denote different $K_p$ conditions (red:$K_p \leq 3$, blue:$K_p \geq 5$) and stand in a horizontal line, ordered from the left-hand side, (1)$10 \leq PE < 100$ eV, (2) $0.1 \leq PE < 1.0$ keV, (3) $1.0 \leq PE < 10.0$ keV, and (4) $PE \geq 10.0$ keV.

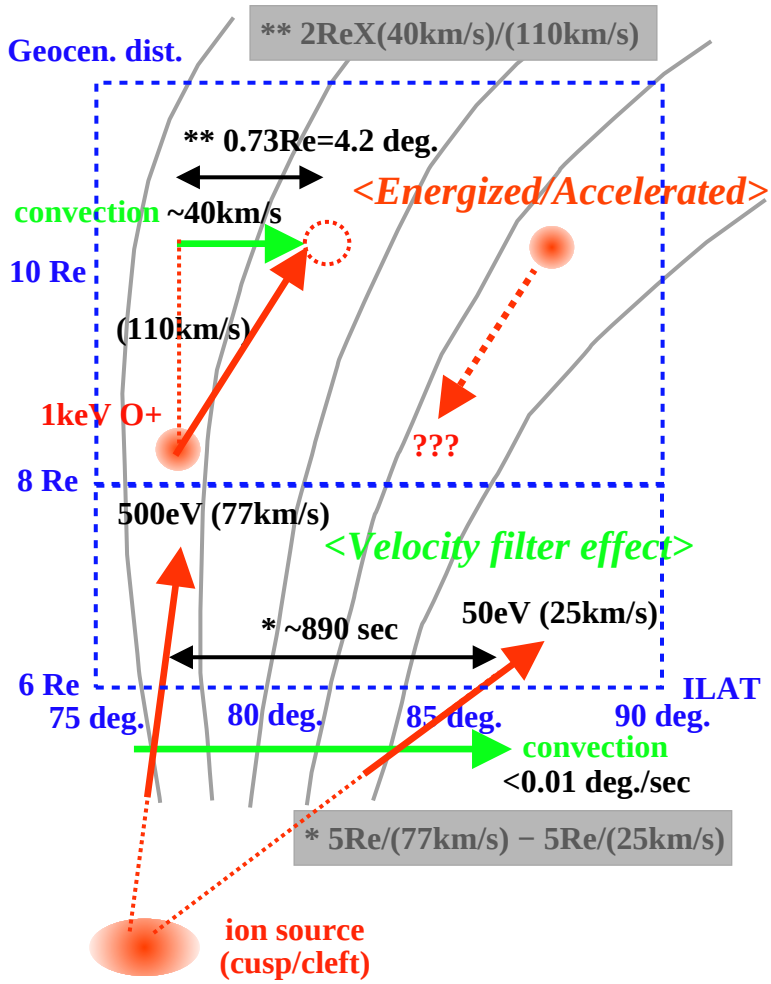


Figure 3.3: Not-scaled schematic interpreting Fig. 3.2. This sketch shows that latitudinal distribution of outflowing $O^+$ observed below 8 $R_E$ geocentric distance can be explained by velocity filter effect, while the distribution above 10 $R_E$ geocentric distance cannot be explained by the velocity filter effect only. Thus we suggest that additional energization/acceleration takes place at such high altitudes and high latitudes. Note that $K_p$ dependence is not taken into account in this sketch.

## 3.3 Solar wind influence on both the magnetosphere and the ionosphere

### 3.3.1 Overview

As mentioned in Paper II, we found higher $K_p$ dependence seen in the appearance of outflowing keV $O^+$ observed in the high-altitude and high-latitude polar region. It is said in general that $K_p$ index indicates planetary-level disturbances closely tied to the solar winds. Furthermore, $K_p$ index is a three-hour averaged value over $K$ values from several stations. Therefore, we aim to clarify the relationships between the appearance of outflowing keV $O^+$ in the high-altitude and high-latitude polar region and the solar wind parameters (including the IMF conditions) and geomagnetic activity (e.g. $ASY/SYM$ indices) in a shorter time scale than 3 hours. We aim also to examine the relationships between both the solar wind parameters / the IMF conditions and $K_p$ index in the same time scale. In addition to these, owing to the good time resolution of data set, we can investigate temporal changes of the former relationships.

The data set concerning the properties of outflowing $O^+$ is the same as which is dealt in Paper II, however the maximum differential particle flux ($MDPF$) of outflowing $O^+$ is dealt with apparently in Paper III. There has been no or very few studies investigating statistically the relationship between the energy of outflowing $O^+$ observed in such high-altitude and high-latitude polar regions on which we have focused and the solar wind parameters / the IMF conditions, while there have been many studies concerning upward flow rate or moments (e.g. density) of outflowing $O^+$. We chiefly look at the energies ($PE$s) of outflowing $O^+$ incidental to 'dominant' or maximum differential particle flux. That is why we also look at $MDPF$ instead of flow rate.

At high-altitude and high-latitude dayside regions (the altitude intervals of 6-12 $R_E$ geocentric distance and the latitude intervals of 75-90 deg ILAT), spatial distribution of $PE$ occurrence rates seem to have an altitude dependence as reported in Paper II, there has been no systematic investigation relevant to such an issue previously. Moreover, such investigations have dealt with stationary conditions, i.e. comparisons between the time-averaged properties of outflowing $O^+$ and the time-averaged solar wind parameters in long, typically an hour, time scales. There is no corresponding high time-resolution index to $K_p$ index, thus we have made use of $ASY/SYM$ indices. These indices almost correspond to 1-minute time resolution $AE$ index and $D_{st}$ index, respectively, therefore these indices are not exactly tied to the solar winds. However, investigating relationships between the properties of outflowing $O^+$ and these geomagnetic activity indices may give us an insight into the inner magnetospheric dynamics via outflowing ionospheric ions.

In Paper III, the relationship between unknown energization/acceleration of dayside high-altitude and high-latitude outflowing $O^+$ (Paper II) and solar wind influence is examined in terms of specifying the location. The outflow process

and energization/acceleration process acting on dayside high-altitude polar outflowing $O^+$ might be differently controlled by the solar winds in terms of response time to the solar winds and the location, which is shown in Paper III. How outflowing $O^+$ observed in the dayside high-altitude polar region correlate to the geomagnetic activity both spatially and temporally is also answered in Paper III.

We examined relationships (correlations) between the properties of outflowing $O^+$ (namely, $PE$ and $MDPF$), the solar wind parameters (including the IMF conditions), and geomagnetic activity. This study is a succession to the previous study (Paper II), therefore the same data set was utilized concerning the properties of outflowing $O^+$. Not only spatial correlations, but also temporal correlations in the time scale (for time lags) ranging from tens of minutes to an hour were investigated.

### 3.3.2 Summary of Paper III

We found, first, that energization/acceleration of outflowing keV $O^+$ is directly controlled by both the solar wind moments (solar wind proton density, $N_p$, solar wind velocity x-component, $V_x$, and solar wind dynamics pressure, $P_{sw}$) and the IMF conditions (strong southward IMF, $B_t$ ($|\theta|>135°$)), however, the places where the influences can be seen are different for the solar wind moments and the IMF conditions. In the poleward part of the cusp and the mantle and only at high altitudes (above 10 $R_E$) the IMF has an influence on observed energies (typically more than 1 keV). In the entire polar cap and above 8 $R_E$ the solar wind moments have the closest influence. Since the optimum time lag for the best correlation was estimated to be approximately 10 minutes, the solar wind influence on energization/acceleration of outflowing keV $O^+$ seems to be almost immediate.

Second, we found that the dayside high-altitude and high-latitude outflow process of $O^+$ in terms of flux enhancement also correlate well with both the solar wind moments ($N_p$, $P_{sw}$, and solar wind electric field, $E4$) and the IMF conditions (strong southward IMF, $B_t$ ($|\theta|>135°$)), however, the solar wind control on the $O^+$ outflow process is predominantly seen very close to the pole in the polar cap (above 85 deg ILAT). Furthermore, the optimum time lag for the best correlation was found basically to be about 60 minutes and the correlation was obvious at lower altitudes (below 8 $R_E$) at the time lag of 60 minutes. This indicates that outflow process (flux enhancement) of $O^+$ in the dayside high-altitude and high-latitude region is closely related to dynamics of the ionosphere as can be expected. Surprisingly, there is no clear correlation between the energization/acceleration of outflowing $O^+$ observed in the dayside high-altitude and high-latitude region, and the solar wind electric field ($E4$). However, $E4$ plays a role on flux enhancement of outflowing $O^+$, as expected from the other previous studies.

Correlations between the properties of outflowing $O^+$ and local low-/mid-

latitude geomagnetic activity are also shown in Paper III. Both energy and flux enhancement of dayside high-altitude polar outflowing $O^+$ correlate to magnitudes of $SYM$-$H$ and $ASY$-$D$. However, correlations to geomagnetic activity are not as clear as the case of solar wind influence. Higher energy of outflowing $O^+$ appears at higher altitudes and more equatorward for higher geomagnetic activity. This trend has also been seen for higher $K_p$. On the other hand, flux enhancement of outflowing $O^+$ appears at lower altitudes and more poleward for higher geomagnetic activity, as measured by $SYM$-$H$ and $ASY$-$D$.

### 3.3.3 On the 3-hour average

Concerning the correlations between 3-hour-averaged solar wind parameters and $K_p$ index, all parameters ($N_p$, $V_x$, $P_{sw}$ and $E4$) show good (and positive) correlations to $K_p$ (linear Person correlation coefficients, $R$, are more than 0.73), in particular the maximum $R$ is 0.92 for the solar wind velocity x-component ($V_x$) (See Fig. 3.4). These results are basically consistent with other previous studies, except best correlation for the solar wind velocity is newly obtained in our study. Regarding the correlation between the IMF (intensity and orientation) and the $K_p$ value, the IMF projection onto $YZ_{gsm}$ plane, $B_t$, seems not to be related to $K_p$ independent of the IMF orientation (southward or northward, defined by clock angle, $\theta$) (Fig. 3.5). However, higher $K_p$ (e.g. $K_p$>6) seems to be associated with the increase of IMF intensity. Note that 3-hour averaged IMF orientations are only considered, not the stationary and/or fluctuated condition. On the other hand, as the average-over-a-given-$K_p$ of standard deviation (SD) on the IMF clock angle increases, $K_p$ also increases (Fig. 3.6). This implies that the IMF variation, rather than its intensity, plays an important role in driving a planetary geomagnetic disturbance.

(a) SW proton density ($N_p$) (b) SW dynamic pressure ($P_{sw}$)

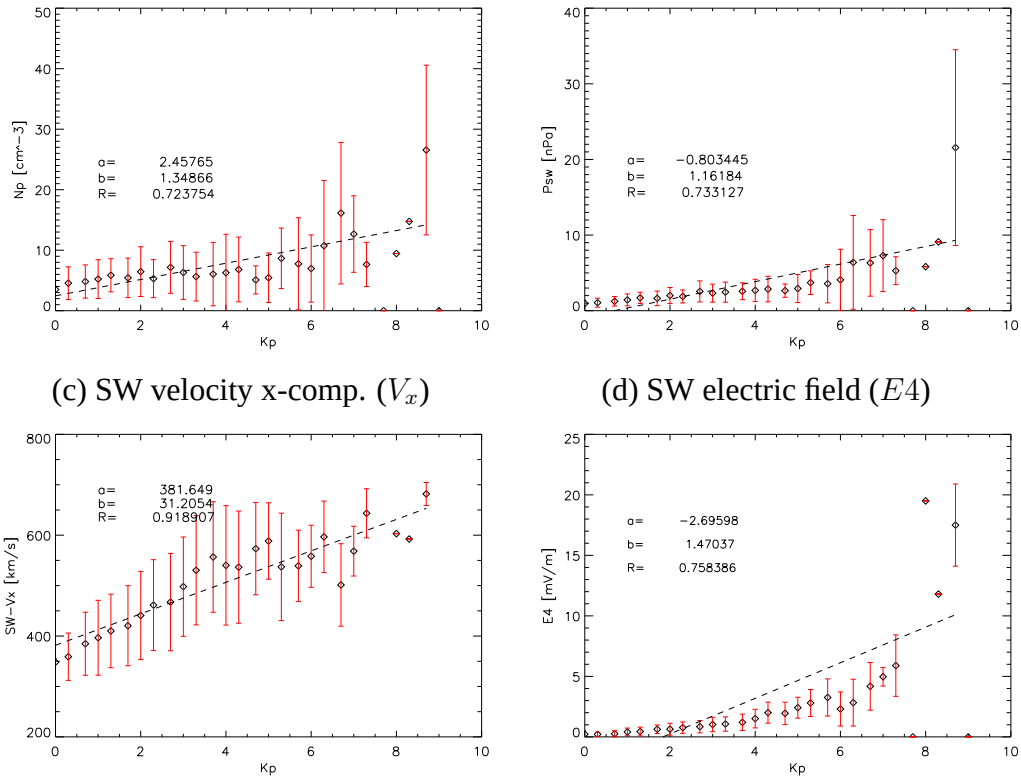


(c) SW velocity x-comp. ($V_x$) (d) SW electric field ($E4$)




Figure 3.4: $K_p$ (horizontal axis) versus the solar wind parameters. The solar wind parameters shown in the panels (from the top, left to right) are (a) solar wind proton density ($N_p$), (b) solar wind dynamic pressure ($P_{sw}$), (c) solar wind velocity x-component ($V_x$), (d) solar wind electric field ($E4$). The 3-hour averaged ACE data are utilized and $K_p$-related averages and standard deviations (SD) of the solar wind parameters are derived. The data are fitted to the linear model, $y = a + bx$, and the linear Pearson correlation coefficients ($R$) are computed.

(a) $B_t$ for southward IMF (b) $B_t$ for northward IMF

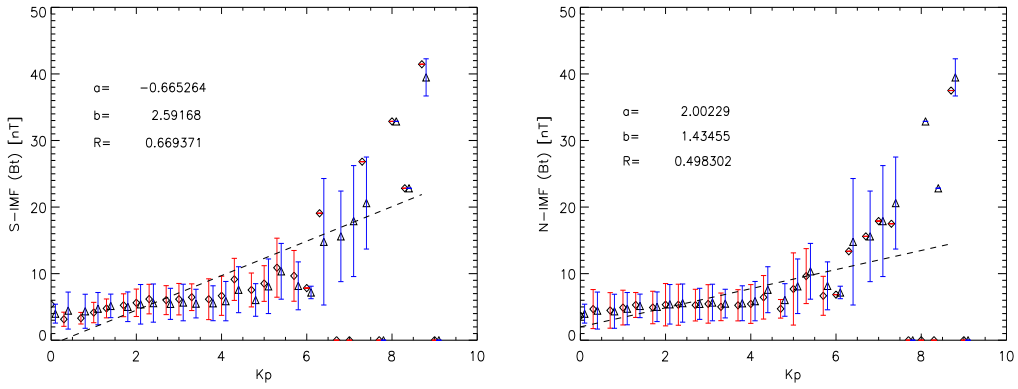


Figure 3.5: $K_p$ (horizontal axis) versus the IMF projection onto the $YZ_{gsm}$ plane ($B_t$). (a) $B_t$ (intensity) for southward IMF (3-hour averaged, fluctuations during 3-hour period are not considered) ($\diamond$ with red error bar), (b) $B_t$ for northward IMF (same style as (a)), and the mark $\triangle$ with blue error bar represents $B_t$ for arbitrary orientations of IMF. As shown in the figures, intensity of the IMF seems not to be related to $K_p$ independent of the IMF orientation, except for higher $K_p$, e.g. $K_p$>6.

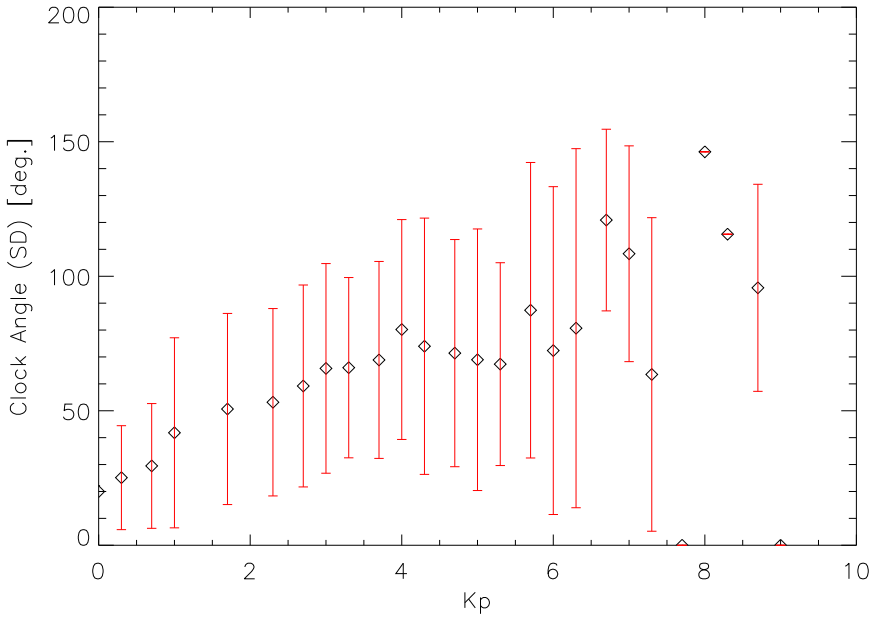


Figure 3.6: $K_p$ (horizontal axis) versus the standard deviation (SD for 3-hour average of ACE data) on IMF clock angle ($\theta$). The SDs are averaged over a given $K_p$ value.

## 3.4 Summary of this thesis

We have found evidences of additional energization/acceleration processes that have never been reported in the dayside high-altitude and high-latitude region. One is a shell-like distribution which has never been observed inside the magnetopause previously. The other is the parallel accelerated (as well as energized) ions which are statistically confirmed through a series of this thesis' works.

# Chapter 4

# Future perspective

This year (2005) is the 5th anniversary for the Phoenix/Cluster mission, and the Cluster project has succeeded in surveying the Earth's magnetosphere and providing good quality of data. However, the more data we obtain from the satellite(s), the more we realize there are unanswered scientific questions on the space plasma (or magnetospheric) physics. Even limited to the Cluster data and relevant to our works presented in this thesis, we have left many unanswered questions behind us:

1. We should identify the dayside high-altitude and high-latitude energization/acceleration process(es) acting on outflowing ionospheric $O^+$: how large (how much) does process influence on the magnetospheric dynamics?, what is the upper energy which $O^+$ can obtain in the process?,

2. We have looked at maximum differential particle flux and its enhancement. Next we should examine the flow rate [$s^{-1}$] on basis of the same observation region. Hence we can also estimate how much the dayside $O^+$ outflows contribute to the total outflows from the Earth,

3. In addition to point 2 above, we may be able to estimate the 'loss' rate of outflowing $O^+$ in the magnetosheath.

The list above is basically (and realistically) investigable using the Cluster data, or in conjugation with other satellite(s) (e.g. Double Star satellite). The list above is focused mainly on the high-altitude magnetosphere, sometimes very close to the boundary (magnetopause)/external interaction (magnetosheath) region, so that we can also be involved in investigating other physical processes that have not been dealt with in this thesis, e.g. discontinuities, diffusion processes, macroscopic turbulence.

Anyway, there are two directions that should be advanced upon in frontiers of knowledge on terrestrial origin $O^+$: to investigate the total circulation process or 'fate' of terrestrial origin $O^+$ in the Earth's magnetosphere, and to investigate magnetospheric dynamics and magnetosphere-ionosphere coupling using terrestrial origin $O^+$ ions as a probe.

# Appendix A

## Some basic concepts and formulae

### A.1 Scale height

The *scale height* ($H$) for an isothermal atmosphere with atoms of mass $m_n$ and temperature $T_n$ is defined as

$$H = k_B T_n / m_n g \tag{1}$$

where $k_B$ is the Boltzmann's constant ($1.38 \cdot 10^{-23}$ J/K) and $g$ is the gravitational acceleration.

### A.2 Adiabatic invariants – Guiding center motion of single particle

For particles in magnetic fields, an *adiabatic invariant* is associated with each of three types of motions, (1) the gyration motion around $\boldsymbol{B}$, (2) the longitudinal motion along $\boldsymbol{B}$, and (3) the drift motion perpendicular to $\boldsymbol{B}$. Regarding *mirror folding effect* by diverging geomagnetic fields, the concept (1) is very important.

**First adiabatic invariant**

This invariant is associated with the cyclotron motion (gyration) of the particle. Here we derive the first invariant by a simple way instead of the approach for canonical momentum of charged particles. In general, the force on a particle along $\boldsymbol{B}$ can be written as

$$F_{\parallel} = \frac{m d\boldsymbol{v}_{\parallel}}{dt} = -\mu \frac{\partial B}{\partial \boldsymbol{s}} = -\mu \bigtriangledown_{\parallel} B \tag{2}$$

where $s$ is along $\boldsymbol{B}$, $\mu (\equiv m v_{\perp}^2 / 2B)$ is the *magnetic moment*. Multiply each side of Eq. 2 by $v_{\parallel} = ds/dt$. The Eq. 2 becomes

$$\frac{d}{dt}\frac{m v_{\parallel}^2}{2} = -\mu \frac{\partial B}{\partial s}\frac{ds}{dt} = -\mu \frac{dB}{dt}. \tag{3}$$

The condition that $\boldsymbol{B}$ is not time-dependent is considered here, thus the convective term of $dB/dt$ is remained, i.e. $dB/dt = \partial B/\partial t + (\boldsymbol{v} \cdot \bigtriangledown) B = v \partial B / \partial s$.

Conservation of the total energy of the particle requires

$$\frac{d}{dt}\left(\frac{1}{2}mv_{\parallel}^2+\frac{1}{2}mv_{\perp}^2\right)=\frac{d}{dt}\left(\frac{1}{2}mv_{\parallel}^2+\mu B\right)=0. \tag{4}$$

Combining Eq. 3 and 4 and obtain

$$-\mu\frac{dB}{dt}+\frac{d}{dt}\left(\mu B\right)=0. \tag{5}$$

The differentiation of the second term results in

$$B\frac{d\mu}{dt}=0. \tag{6}$$

Since $B \neq 0$, the Eq. 6 implies that the magnetic moment $\mu$ is independent of time and is a constant in the guiding center motion, moreover that the total magnetic flux enclosed by the motion must also remain constant. The concept of first invariant leads to *magnetic trapping* of particles and the magnetic moment ($\mu$) is conserved as long as the perturbation time scale is much longer than the cyclotron period.

## A.3 Maxwellian distributions

Many of the characteristic features of plasmas can be understood by knowing a specific property of the distribution function, i.e. a reduced six-dimensional phase space distribution function or simply *velocity distribution function*, assuming the plasma to be spatially homogeneous (or dependent on the velocity at a fixed position) and stationary (time-independent). The conditions in which the plasma does not change in time and does not exhibit spatial variations can be realized when the plasma is in equilibrium. The general equilibrium velocity distribution function of a collisionless plasma is called the *Maxwellian velocity distribution* or *Maxwellian* in simple.

$$\begin{aligned} f(\boldsymbol{x},\boldsymbol{v},t) &\rightarrow f(\boldsymbol{v}), \\ f(\boldsymbol{v}) &= n\left(\frac{m}{2\pi k_B T}\right)^{3/2} exp\left(-\frac{m|\boldsymbol{v}|^2}{2k_B T}\right) \end{aligned} \tag{7}$$

where $n$ is the particle number density, $m$ is the particle mass, $k_B$ is the Boltzmann constant (=1.38·10$^{-23}$ J/K), and $T$ is the particle temperature. Besides $k_B T$ denotes the average thermal energy and the velocity spread, $\langle v\rangle = (2k_B T/m)^{1/2}$, can be identified as the *thermal velocity*.

A Maxwellian plasma in thermal equilibrium implies that (a) it does not contain any free energy, hence (b) there are no energy exchange processes between the particles in the plasma, and (c) the velocities of particles are distributed randomly around the average velocity which is zero for a rest frame of plasmas.

## A.4 Differential particle flux

The *differential particle flux,* $J(W, \alpha, \boldsymbol{x})$, per unit area at a given energy ($W$), pitch angle ($\alpha$), and position ($\boldsymbol{x}$), can be described in terms of the particle phase space distribution, $f(\boldsymbol{v}, \boldsymbol{x})$.

Considering the particles found in a velocity interval $dv$ coming from a solid angle $d\Omega$, the particle number flux with velocity $v$ across a surface in a phase space volume element ($vdn$=$fv^3 dv d\Omega$) is

$$J(W, \alpha, \boldsymbol{x}) dW d\Omega = f(v_{\parallel}, v_{\perp}, \alpha, \boldsymbol{x}) v^3 dv d\Omega. \tag{8}$$

Since $dW$=$mvdv$, thus the Eq. 8 becomes

$$J(W, \alpha, \boldsymbol{x}) = \frac{v^2}{m} f(v_{\parallel}, v_{\perp}, \alpha, \boldsymbol{x}). \tag{9}$$

# Appendix B

## Some key physical mechanisms and processes

### B.1 Centrifugal Acceleration

The parallel acceleration, $dv_{\parallel}/dt$, derived from the equation of a guiding-center motion has the term of magnetic field curvature-related acceleration associated with the convection,

$$\frac{dv_{\parallel}}{dt} = \boldsymbol{V}_{\boldsymbol{E}\times\boldsymbol{B}} \cdot \frac{d\hat{\boldsymbol{b}}}{dt} = \boldsymbol{V}_{\boldsymbol{E}\times\boldsymbol{B}} \cdot \left\{ \frac{\partial \hat{\boldsymbol{b}}}{\partial t} + \left( v_{\parallel} \frac{\partial}{\partial s} + \boldsymbol{v} \cdot \bigtriangledown \right) \hat{\boldsymbol{b}} \right\} \qquad (10)$$

where $\boldsymbol{V}_{\boldsymbol{E}\times\boldsymbol{B}}$ is the $\boldsymbol{E}\times\boldsymbol{B}$ drift velocity, $\hat{\boldsymbol{b}}$ is the unit vector of geomagnetic field ($\boldsymbol{B}/|\boldsymbol{B}|$), and $s$ is along the geomagnetic field line. The second term on the right-hand side corresponds to acceleration or deceleration due to diverging or converging geomagnetic fields, and the third term corresponds to the centrifugal effect from the curved field lines ($\bigtriangledown \hat{\boldsymbol{b}} \equiv -\boldsymbol{\rho}/\rho^2$, where $\boldsymbol{\rho}$ is the radius vector of curvature, and $\boldsymbol{v} \approx \boldsymbol{v}_{\perp}$ can be replaced by $\boldsymbol{V}_{\boldsymbol{E}\times\boldsymbol{B}}$). As is obvious from Eq. 10, the second term is proportional to both field-aligned and drift velocities, while the third term is proportional only to the square of drift velocity. Therefore, the centrifugal acceleration is very effective under such conditions that the convection is enhanced and the geomagnetic field lines are curved, e.g. from the poleward cusp and/or the mantle toward the polar cap where the open field lines are bent tailward. The importance of this mechanism associated with the polar wind acceleration has been studied by *Cladis* (1986) and *Horwitz et al.* (1994a).

### B.2 Ponderomotive force

A ponderomotive force exerted by electromagnetic waves is one of several possible mechanisms of particle acceleration. Inhomogeneous (i.e. expected to be non-resonant) electromagnetic waves of large temporally varying amplitude exert a radiation pressure onto plasmas (therefore, e.g. "magnetic moment pumping" by *Lundin and Hultqvist* (1989) is a kind of ponderomotive force). The pressure force exerted by a wave field such as ponderomotive force is defined as

$$\boldsymbol{f} = -\frac{1}{2n_0} \bigtriangledown W_w \tag{11}$$

where $W_w$ is the wave energy density which is divided by the number density ($n_0$) in order to obtain the force acting on one particle. The relation between the wave energy density ($W_w$) and the electric field energy density is given by

$$W_w = \frac{\partial(\omega\epsilon)}{\partial\omega} W_E \tag{12}$$

where $W_E$=$(\varepsilon_0/2)|\delta\mathsf{E}|^2$ ($\varepsilon_0$ is the dielectric constant in vacuum and $\delta\mathsf{E}$ is the pump wave field), and $\epsilon$ is the dielectric function which is given as $\epsilon(\omega)$=$1 - \omega_{pe}^2/\omega^2$) ($\omega_{pe}$ is the electron plasma frequency).

Therefore, the ponderomotive force is formulized as below when assuming constant $\epsilon$,

$$\begin{aligned} \boldsymbol{f} &= \frac{\epsilon - 1}{2n_0} \bigtriangledown W_E, \\ &= -\frac{\varepsilon_0 \omega_{pe}^2}{4n_0\omega^2} \bigtriangledown |\delta\mathsf{E}|^2. \end{aligned} \tag{13}$$

From the observational point of view, in the cusp and polar cap boundary where inverted-V electrons are usually not present, and it is difficult to identify a distinct current direction. For the wave-heating mechanisms it is usually said that the currents and/or the ion and electron beams are necessary to excite instabilities, then these drive the necessary wave modes to heat ions through cyclotron resonance. In the region mentioned above (cusp and polar cap), Alfvén waves are a nearly permanent feature (*Chaston et al.*, 2003a, 2004). The ponderomotive force is a possible mechanism by which Alfvén waves with frequency $\omega \ll \Omega_i$ (ion cyclotron frequency) and perpendicular wave number $k_\perp \ll 2\pi/\rho_i$ (inverse ion gyroradius) may accelerate ions.

# Appendix C

## $X$ distance method and the solar wind parameters

### C.1 Maximum error estimation associated with the $X$ distance method

The IMF and solar wind (bulk) parameters (or moments) are distributed by, e.g. the ACE (Advanced Composition Explorer) spacecraft which is located at around the L1 point and upstream of the magnetosphere ($\sim$220 $R_{\mathsf{E}}$). Therefore the propagation time, $t_{swp}$, of the solar wind to reach the magnetosphere (i.e. the subsolar magnetopause) is calculated by means of the $X$ distance method.

One-point (one spacecraft) observation is not enough to estimate the propagation time of more precise, because it lacks of the information about how the solar wind leading-edge (in analogy to a two-dimensional plain wave) inclines against to the Sun-Earth line, thus no one can know to what part of the magnetosphere the solar wind encounters. However, for the purpose of my thesis study, such a precision to estimate the propagation time is not required. Therefore, the data from one-point observation is utilized.

We also utilize the same technique as in the work by *Collier et al.* (1998) to estimate the maximum error associated with the $X$ distance method. The timing uncertainty $\Delta t$ given an estimated solar wind propagation time $t_{swp}$ (using the average solar wind speed over the interval), a separation from the Sun-Earth line of $d_{\perp}$, and a distance upstream from the magentopause $d_{\parallel}$ are given the following relation

$$\Delta t \sim (d_{\perp}/d_{\parallel}) \cdot t_{swp}. \tag{14}$$

For example, from the data set of ACE/SWEPAM during January to May, 2001–2003, the average solar wind velocity x-component ($V_x$) is $\sim$430 km/s at the ACE observation point, thus

$$\frac{1}{< V_x >} = \frac{< t_{swp} >}{< d_{\parallel} >} = 1/430[s/km] = 0.25[min/R_{\mathsf{E}}]. \tag{15}$$

The transverse separation along the Sun-Earth line ($d_{\perp}$) is calculated as 39 $R_{\mathsf{E}}$ on the average during the same period, therefore the maximum error for the solar wind propagation time is estimated as 0.25(min/$R_{\mathsf{E}}$)$\times d_{\perp}$(=39 $R_{\mathsf{E}}$)$\approx$10 minutes.

## C.2 The solar wind parameters and the IMF

Regarding the solar wind parameters (moments) that are available from the 2-level 64-second averaged ACE data, we look at (1) the solar wind proton density ($N_p$), (2) the solar wind dynamic pressure ($P_{sw}$=$N_p m_p V_{sw}^2$ where $m_p$ is mass of proton and $V_{sw}$ is solar wind velocity), (3) the IMF $B_{x,gsm}$ (hereafter $B_x$), (4) the IMF projection onto $YZ_{gsm}$ plane ($B_t$), (5) the clockwise angle between $B_t$ and the positive $Z_{gsm}$ direction (in short, the IMF clock angle, and $\theta$), (6) the solar wind velocity x-component in GSM coordinate ($V_{sw,x}$, but hereafter $V_x$). With respect to (4) and (5) above, $B_t$ and $\theta$ are adopted on account of usefulness instead of $B_y$ and $B_z$.

In addition to the solar wind parameters mentioned above, we also introduce the model reconnection electric field (or solar wind (convective) electric field), $E4$=$|V_x||B_t|sin^4(\theta/2)$ (***Eriksson et al.***, 2001). This quantity is originally introduced by *Akasofu* (1981) as the power $\epsilon$, and

$$\epsilon = VB^2 sin^4\left(\frac{\theta}{2}\right) l_0^2 \tag{16}$$

where $l_0$=constant($\sim$7 $R_E$). Hence, here it is simplified only to show the combined effect by the $X_{gsm}$ direction solar wind velocity and the IMF $B_z$.

# Appendix D

## Geomagnetic indices

The magnetic fields measured by ground-based observatories are distributed by either the ($H$, $D$, $Z$) or the ($X$, $Y$, $Z$) coordinate system. The $H$-component represents the horizontal component of the magnetic field tangent to the surface. The $Z$-component represents the vertical component defined as positive in the downward (toward the center of Earth) direction. The $D$-component is the declination measured from true north (positive for eastward). The relationships between both components are

$$\begin{aligned} X &= HcosD, \\ Y &= HsinD, \\ Z &= Z. \\ &or \\ B_\lambda &= +X, \\ B_\phi &= +Y, \\ B_r &= -Z. \end{aligned} \tag{17}$$

The following description of several indices in details can be found, for example, via World Data Center for Geomagnetism, Kyoto.
(`http://swdcdb.kugi.kyoto_u.ac.jp/wdc/Sec3.html`).

### D.1 $K_p$ index

The following definition of "K variations" has been given by *Siebert* (1971):

> *K variations are all irregular disturbances of the geomagnetic field caused by solar particle radiation within the 3-h interval concerned. All other regular and irregular disturbances are non K variations. Geomagnetic activity is the occurrence of K variations. (original in German)*

Local disturbance levels are determined by measuring the range (difference between the highest and lowest values) during three-hourly time intervals for the most disturbed horizontal magnetic field component. First, however, the quiet-day variation pattern has to be removed from the magnetogram, a somewhat

subjective procedure.

Thus $K_p$ is a 'quantitative' measure of the planetary disturbance level, ranging from 0 to 9 with plus and minus intermediate (sub)levels at each given level (e.g. $1^-$, 1, $1^+$). The scale of $K_p$ is quasi-logarithmic due to station specific (the corresponding linear index is $A_p$) and is based on 'local' $K$ indices from the 13 selected stations, which are collected and regional peculiarities are removed.

More precisely, $K$ index still remains a local index, describing disturbances in the vicinity of each observatory. Therefore, by applying the "conversion tables", a standardized index $K_s$ for each of the 13 selected observatories is determined. These conversion tables were generated by means of statistical methods to eliminate an annual cycle of daily variations attributed to the geographic and geomagnetic coordinates of each observatory.

The 13 selected observatories lie between 49 to 62 degrees geomagnetic latitudes in the northern hemisphere (11 stations), between -43 to -47 degrees geomagnetic latitudes in the southern hemisphere (2 stations).

## D.2 $D_{st}$ index

The ring current index $D_{st}$ is introduced as a measure of the ring current magnetic field (developments/decays). The $D_{st}$ index represents the average disturbance field at the Earth's equator and is calculated on the basis of observations from four low-latitude magnetic observatories (Honolulu, San Juan, Hermanus, and Kakioka). The $D_{st}$ index is calculated as

$$D_{st} = \frac{1}{16}\left(\sum_{i=1}^{4} cos\Lambda_i\right) \cdot \left[\sum_{i=1}^{4} H(t) - H_0(t^{'}) - H_{sq}(t^{'})\right]_i \qquad (18)$$

where subtracting a quiet time reference level ($H_0(t^{'})$) and the $Sq$ field ($H_{sq}(t^{'})$), which both vary with local time $t^{'}$, from the hourly averaged measured $H$ component, then all four magnetic disturbances are averaged to reduce local time effect and multiplied with the averages of the cosines of the observatories' dipole latitudes, $\Lambda_i$, to obtain the hourly averaged $D_{st}$ index at universal time $t$.

By the way, the solar radiation heating the atmosphere excites the tides with diurnal or semi-diurnal oscillations. The ionospheric current system created by this tidal motion of the atmosphere is called *solar quiet current* ($Sq$ current).

The uncertainties of $D_{st}$ are mainly caused by other $H$ component disturbances raised in magnetopause current, the (westward) partial ring current prevailing in the afternoon sector, and the substorm current wedge dominating in the midnight and early morning sector. The magnetopause current is controlled by the solar wind pressure and its magnetic perturbation peaks around noon (Experimentally the maximum uncertainty becomes 50% of a $D_{st}$ value of 50 nT around noon, while the uncertainty is relatively small in the nightside).

The coordinates of observatories are given in Table 1.

Table 1: The coordinates of observatories ($D_{st}$)

| Observatory | Geomagnetic dipole latitude [°] |
|---|---|
| Hermanus | -33.3 |
| Kakioka | 26.0 |
| Honolulu to April 1960 | 21.0 |
| Honolulu after April 1960 | 21.1 |
| San Juan to January 1965 | 29.9 |
| San Juan after January 1965 | 29.9 |

## D.3 $AE$ index

The auroral electrojet $AE$, $AU$ and $AL$ are introduced as a measure of global auroral electrojet activity. These indices are based on the measurement of northward $H$-component from twelve auroral zone observatories located between 65° and 70° magnetic latitude with a longitudinal spacing 10-40°. The indices are calculated as

$$\begin{aligned} AU(t) &= \max_{i=1,12} [H(t) - H_0]_i \\ AL(t) &= \min_{i=1,12} [H(t) - H_0]_i \\ AE(t) &= AU(t) - AL(t) \end{aligned} \tag{19}$$

where $t$ is universal time.

The main uncertainties of the $AE$ index stem, one from the effects of strong field-aligned currents, on the other hand, the other from the locations of observatories. A long longitudinal gap corresponding to missing the two-hour local time measurement cannot cover substorm current wedges associated with weak and moderate substorms continuing less than two hours. Furthermore, the small latitudinal range covered by the $AE$ observatories, in particular located south of 70°, cannot detect the maximum disturbances when the IMF is northward directed and convection ceases and consequently the auroral oval contracts northward and the electrojets tend to flow poleward of 70° latitude.

The geomagnetic coordinates of $AE$ 12 observatories lie between 60 to 71 degrees.

## D.4 $ASY/SYM$ indices

The $ASY$ indices indicate the effects of such as the asymmetric (or 'partial') ring current, the field-aligned currents or the substorm current wedge. *Iyemori and Rao* (1996) have used both $ASY$-$H$ and $ASY$-$D$ indices to determine the onset time of a substorm, as well as a sharp decrease in the $AL$ index. A substorm activity is defined as a polar region process which is characterized by a sudden

Table 2: The coordinates of observatories ($ASY/SYM$ indices)

| Observatory | Geomagnetic latitude [°] | Invariant latitude [°] |
|---|---|---|
| San Juan | 29.1 | 32.5 |
| Fredericksburg | 49.1 | 50.4 |
| Boulder | 48.7 | 49.1 |
| Tucson | 40.4 | 39.7 |
| Honolulu | 21.5 | 20.2 |
| Memambetsu | 34.6 | 34.9 |
| Alibag | 9.9 | – |
| Martin de Vivies | -46.9 | 48.6 |
| Hermanus | -33.7 | 43.6 |
| Chambon-la-Foret | 50.1 | 45.7 |

auroral electrojet intensification indicated by the $AE$ indices.

The $SYM$-$H$ index is, on the other hand, a measure of a symmetric part of geomagnetic field disturbance for the component in horizontal (dipole) direction, and essentially the same as $D_{st}$ index except for time resolution (1-minute time resolution for $SYM$-$H$ and hourly average for $D_{st}$). The $D_{st}$ field development (i.e. $SYM$-$H$ decrease) indicates the equatorial ring current development (enhancement), which causes a large decrease in the horizontal component of geomagnetic field at mid-/low-latitudes. This phenomenon is generally defined as a geomagnetic storm.

In Table 2, geomagnetic and invariant latitudes of observatories are given.

# Bibliography


Abe, T., Whalen, B. A., Yau, A. W., Horita, R. E., Watanabe, S. and Sagawa, E.: EXOS-D (Akebono) superthermal mass spectrometer observations of the polar wind, *J. Geophys. Res.*, 98, 11191–, 1993a.

Abe, T., Whalen, B. A., Yau, A. W., Watanabe, S., Sagawa, E. and Oyama, K. I.: Altitude profile of the polar wind velocity and its relationship to ionospheric conditions, *Geophys. Res. Lett.*, 20, 2825–, 1993b.

Akasofu, S.-I.: Energy coupling between the solar wind and the magnetosphere, *Space Sci. Rev.*, 28, 121–, 1981.

Alfvén, H.: On the theory of magnetic storms and aurorae, *Tellus*, 10, 104–, 1958.

Arvelius, S., Yamauchi, M., Nilsson, H., Lundin, R., Hobara, Y., Rème, H., Bavassano-Cattaneo, M. B., Paschmann, G., Korth, A., Kistler, L. M., and Parks, G. K.: Statistics of high-altitude and high-latitude $O^+$ ion outflows observed by Cluster/CIS, *Ann. Geophys.*, 23, 1909–1916, 2005.

Arvelius, S., Yamauchi, M., Nilsson, H., Lundin, R., Rème, H., Bavassano-Cattaneo, M. B., Paschmann, G., Korth, A., Kistler, L. M., and Parks, G. K.: Statistical study of relationships between dayside high-altitude and high-latitude $O^+$ ion outflows, solar winds, and geomagnetic activity, submitted to *Ann. Geophys.*, 2005.

Axford, W. I.: The polar wind and the terrestrial helium budget, *J. Geophys. Res.*, 73, 6855–, 1968.

Banks, P. M. and Holzer, T. E.: The polar wind, *J. Geophys. Res.*, 73, 6846–, 1968.

Banks, P. M. and Holzer, T. E.: High latitude plasma transport: the polar wind, *J. Geophys. Res.*, 74, 6317–, 1969.

Banks, P. M., Schunk, R. W., and Raitte, W. J.: The topside ionosphere: A region of dynamic transition, *Annl. Rev. Earth Planet. Sci.*, 4, 381–, 1976.

Baumjohann, W. and Treumann, R. A.: *Basic Space Plasma Physics*, Imperial College Press, U.K., 1996.

Baumjohann, W. and Treumann, R. A.: *Advanced Space Plasma Physics*, Imperial College Press, U.K., 1996.

Bergmann, R. and Lotko, W.: Transition to unstable ion flow in parallel electric fields, *J. Geophys. Res.*, 91, 7033–7045, 1986.

Block, L. P. and Fälthammar, C.-G.: The role of magnetic-field-aligned electric fields in auroral acceleration, *J. Geophys. Res.*, 95, 5677–, 1990.

Bonnell, J., Kintner, P., Wahlund, J.-E., Lynch, K. and Arnoldy, R.: Interferometric determination of broadband ELF wave phase velocity within a region of transverse auroral ion acceleration, *Geophys. Res. Lett.*, 23, 3297–, 1996.

Brinton, H. C., Grebowski, J. M. and Mayr, H. G.: Altitude variation of ion composition in the mid-latitude through region: Evidence for upward plasma flow, *J. Geophys. Res.*, 76, 3738–, 1971.

Candidi, M., Orsini, S. and Horwitz, J. L.: The tail lobe ion spectrometer, *J. Geophys. Res.*, 93, 14401–, 1988.

Cannata, R. W. and Gombosi, T. I.: Modelling of the solar cycle dependence of quiet-time ion upwelling at high geomagnetic latitudes, *Geophys. Res. Lett.*, 16, 1141–, 1989.

Carlson, C. W., McFadden, J. P., and Mende, S. B.: Electron acceleration and ion outflow in the polar cap boundary region during magnetospheric substorms, *AGU Fall Meeting 2001*, abstract#SM52B-03, 2001.

Chang, T., Crew, G. B., Hershkowitz, N., Jasperse, J. R., Retterer, J. M. and Winningham, J. D.: Transverse acceleration of oxygen ions by electromagnetic ion cyclotron resonance with broadband left-hand-polarized waves, *Geophys. Res. Lett.*, 13, 636–, 1986.

Chaston, C. C., Bonnell, J. W., Carlson, C. W., Ergun, R. E., McFadden, J. P., and Strangeway, R. J.: Properties of small scale Alfvén waves and accelerated electrons from FAST, *J. Geophys. Res.*, 108, 8003–, doi:10.1029/2002JA009420, 2003a.

Chaston, C. C., Bonnell, J. W., Carlson, C. W., Ergun, R. E., McFadden, J. P., Strangeway, R. J., and Lund, E. L.: Auroral ion acceleration in dispersive Alfvén waves, *J. Geophys. Res.*, 109, doi:10.1029/2003JA010053, 2004.

Cladis, J. B.: Parallel acceleration and transport of ions from polar ionosphere to plasma sheet, *Geophys. Res. Lett.*, 13, 893–, 1986.

Collier, M. R., Slavin, J. A., Lepping, R. P., Szabo, A. and Ogilvie, K.: Timing accuracy for the simple planar propagation of magnetic field structures in the solar wind, *Geophys. Res. Lett.*, 25, 2509–2512, 1998.

Cravens, T. E., Hoppe, A., Ledvina, S. A., and McKenna-Lawlor, S.: Pickup ions near Mars associated with escaping oxygen atoms, *J. Geophys. Res.*, 107, 1170–1179, doi:10.1029/2001JA000125, 2002.

Cully C. M., Donovan, E. F., Yau, A. W. and Arkos, G. G.: Akebono/Suprathermal Mass Spectrometer observations of low-energy ion outflow: Dependence on magnetic activity and solar wind conditions, *J. Geophys. Res.*, 108(A2), 1093–, doi:10.1029/2001JA009200, 2003.

Demars, H. G., Barakat, A. R. and Schunk, R. W.: Effect of centrifugal acceleration on the polar wind, *J. Geophys. Res.*, 101(A11), 24565–24571, 1996.

Eklund, U., Lundin, R., and Sandahl, I.: Measurements of $O^+$ in the high latitude magnetosheath, *Phys. Chem. Earth.*, 22, 639–644, 1997.

Eliasson, L., Lundin, R., and Murphree, J. S.: Polar cap acrs observed by the Viking satellite, *Geophys. Res. Lett.*, 14, 451–454, 1987.

Eliasson, L., André, M., Lundin, R., Pottelette, R., Marklund, G., and Holmgren, G.: Observations of electron conics by the Viking satellite, *J. Geophys. Res.*, 101, 13225–13238, 1996.

Elliott, H. A., Comfort, R. H., Craven, P. D., Chandler, M. O. and Moore, T. E.: Solar wind influence on the oxygen content of ion outflow in the high-altitude polar cap during solar minimum conditions, *J. Geophys. Res.*, 106(A4), 6067-6084, doi10.1029/2000JA003022, 2001.

Eriksson, S., Blomberg, L. G., Ivckenko, N., Karlsson, T. and Marklund, G. T.: Magnetospheric response to the solar wind as indicated by the cross-polar potential drop and the low-latitude asymmetric disturbance field, *Ann. Geophys.*, 19, 649–653, 2001.

Evans, D. S.: The observations of a near monoenergetic flux of auroral electrons, *J. Geophys. Res.*, 73, 2315–, 1968.

Fontaine, D., Teste, A., Maggiolo, R., Sauvaud, J.-A., Paschmann, G., and Fazakerley, A. N.: Electron dynamics associated with ion beam acceleration above the polar cap, *AGU Fall Meeting 2004*, abstract#SM13B-1223, 2004.

Frank, L. A., Ackerson, K. L. and Yeager, D. M.: Observations of atomic oxygen ($O^+$) in the Earth's magnetotail, *J. Geophys. Res.*, 82, 129–, 1977.

Fuselier, S. A., Shelley, E. G., and Klumpar, D. M.: AMPTE/CCE observations of shell-like $He^{++}$ and $O^{6+}$ distributions in the magnetosheath, *Geophys. Res. Lett.*, 15, 1333–1336, 1988.

Giles, B. L., Chappell, C. R., Moore, T. E., Comfort, R. H. and Waite, J. H. Jr.: Statistical survey of pitch angle distributions in core (0-50 eV) ions from Dynamic Explorer 1: Outflow in the auroral zone, polar cap, and cusp, *J., Geophys. Res.*, 99, 17483–17501, 1994.

Gorney, D. J., Clarke, A., Croley, D., Fennell, J., Luhmann, J. and Mizera P.: The distribution of ion beams and conics below 8000 km, *J. Geophys. Res.*, 86, 83–, 1981.

Guglielmi, A. and Lundin, R.: Ponderomotive upward acceleration of ions by ion cyclotron and Alfvén waves over the polar regions, *J. Geophys. Res.*, 106(A7), 13219–13236, 2001.

Heelis, R. A., Lowell, J. K. and Spiro, R. W.: A model of the high-latitude ionospheric convection pattern, *J. Geophys. Res.*, 87(A8), 6339–6345, 1982.

Heppner, J. P. and Maynard, N. C.: Empirical high-latitude electric field models, *J. Geophys. Res.*, 92, 4467–, 1987.

Hirahara, M., Mukai, T., Terasawa, T., Machida, S., Saito, Y., Yamamoto, T. and Kokubun, S.: Cold dense ion flows with multiple components observed in the distant tail lobe by Geotail, *J. Geophys. Res.*, 101, 7769–, 1996b.

Ho, C. W., Horwitz, J. L., and Moore, T. E.: DE1 observation of polar $O^+$ stream bulk parameters and comparison with a model of the centrifugally-accelerated polar wind, *Geophys. Res. Lett.*, 21, 2459–2462, 1994.

Hobara, Y., Nilsson, H., Arvelius, S., Lundin, R., Sundkvist, D., André, M., Cornilleau-Wehrlin, N. et al.: Cluster observation of high altitude oxygen outflow burst and associated wave activities, EGU General Assembly (abstract), 2005.

Hoffman, J. H.: Studies of the composition of the ionosphere with a magnetic deflection mass spectrometer. *Int. J. Mass Spect. Ion Phys.*, 4, 315–, 1970.

Hoffman, J. H., Dodson, W. H., Lippincott, C. R. and Hammack, H. D.: Initial ion composition results from the ISIS-2 satellite, *J. Geophys. Res.*, 79, 4246–, 1974.

Hoffman, J. H. and Dodson, W. H.: Light ion concentrations and fluxes in the polar regions during magnetically quiet times, *J. Geophys. Res.*, 85, 626–, 1980.

Horwitz, J. L. and Lockwood, M.: The cleft ion fountain: A two-dimensional kinetic model, *J. Geophys. Res.*, 90, 9749–, 1985.

Horwitz, J. L., Pollock, C. J., Moore, T. E., Peterson, W. K., Burch, J. L., Winningham, J. D., Craven, J. D., Frank, L. A., and Persoon, A.: The polar cap environment of outflowing $O^+$, *J. Geophys. Res.*, 97, 8361–8379, 1992.

Horwitz, J. L., Ho, C. W., Scarbro, H. D., Wilson, G. R. and Moore, T. E.: Centrifugal acceleration of the polar wind, *J. Geophys. Res.*, 99, 15051–, 1994a.

Hultqvist, B.: On the production of a magnetic-field aligned electric field by the interaction between the hot magnetospheric plasma and the cold ionosphere, *Planet Space Sci.*, 19, 749–, 1971.

Hultqvist, B. et al.: On the acceleration of electrons and positive ions in the same direction along magnetic field by parallel electric fields, *J. Geophys. Res.*, 93, 9777–, 1988.

Hultqvist, B., Øieroset, M., Paschmann, G., Treumann, R.: *Magnetospheric Plasma Sources and Losses, Space Science Reviews*, Vol.88, Nos.1–2, 1999.

Iyemori, T. and Rao, D. R. K.: Decay of the Dst field of geomagnetic disturbance after substorm onset and its implication to storm-substorm relation, *Ann. Geophys.*, 14, 608–618, 1996.

Joko, S., Nilsson, H., Lundin, R., Popielawska, B., Rème, H., Bavassano-Cattaneo, M. B., Paschmann, G., Korth, A., Kistler, L. M., and Parks, G. K.: Shell-like configuration in O+ ion velocity distribution at high altitudes in the dayside magnetosphere observed by Cluster/CIS, *Ann. Geophys.*, 22, 2473–2483, 2004.

Klumpar, D. M.: Transversely acceleration ions: An ionospheric course of hot magnetospheric ions, *J. Geophys. Res.*, 84, 4229–, 1979.

Klumpar, D. M., Peterson, W. K. and Shelley, E. G.: Direct evidence for two-stage (bimodal) acceleration of ionospheric ions, *J. Geophys. Res.*, 95, 10779–, 1984.

Lennartsson, O. W., Collin, H. L., and Peterson, W. K.: Solar wind control of Earth's $H^+$ and $O^+$ outflow rates in the 15-eV to 33-keV energy range, *J. Geophys. Res.*, 109, doi:10.1029/2004JA010690, 2004.

Lindqvist, P.-A. and Marklund, G. T.: A statistical study of high-altitude electric fields measured on the Viking satellite, *J. Geophys. Res.*, 95, 5867–5876, 1990.

Lockwood, M., Chandler, M. O., Horwitz, J. L., Waite, J. H. Jr., Moore, T. E. and Chappell, C. R.: The cleft ion fountain, *J. Geophys. Res.*, 90, 9736–, 1985a.

Lundin, R. and Hultqvist, B: Ionospheric plasma escape by high-latitude electric fields: Magnetic moment pumping, *J. Geophys. Res.*, 94, 6665–6680, 1989.

Lundin, R., Gustafsson, G., Eriksson, A. I., and Marklund, G.: On the importance of high-altitude low-frequency electric field fluctuations for the escape of ionospheric ions, *J. Geophys. Res.*, 95, 5905–5919, 1990.

Lundin, R. and Eliasson, L.: Auroral energization processes, *Ann. Geophys.*, 9, 202–, 1991.

Lundin, R., Yamauchi, M., Woch, J., and Marklund, G.: Boundary layer polarization and voltage in the 14 MLT region, *J. Geophys. Res.*, 100, 7587–7597, 1995.

Lundin, R., Hultqvist, B., Dubinin, E., Zackarov, A., and Pissarenko, N.: Observations of outflowing ion beams on auroral field lines at altitudes of many earth radii, *Planet. and Space Sci.*, 30, 715–726, 1982.

Mälkki, A. and Lundin, R.: Altitude distributions of upward flowing ion beams and solitary wave structures in the Viking dat, *Geophys. Res. Lett.*, 21, 2243–, 1994.

Marubashi, K.: Escape of the polar ionospheric plasma into the magnetospheric tail, *Rep. Ionos. Space Res. Jpn.*, 23, 322–, 1970.

Marklund, G. T.: Viking investigations of auroral electrodynamical parameters, *J. Geophys. Res.*, 98, 1691–, 1993.

McIlwain, C. E.: Direct measurement of particles producing visible aurora, *J. Geophys. Res.*, 65, 2727–, 1960.

Miyake, W., Mukai, T. and Kaya, N.: On the origins of the upward shift of elevated (bi-modal) ion conics in velocity space, *J. Geophys. Res.*, 101, 26961–, 1996.

Moore, T. E., Lockwood, M., Chandler, M. O., Waite, J. H. Jr, Chappell, C. R., Persoon, A. and Sugiura, M.: Upwelling $H^+$ ion source characteristics, *J. Geophys. Res.*, 91, 7019–, 1986.

Moore, T. E., Chappell, C. R., Chandler, M. O., Craven, P. D., Glies, B. L., Pollock, C. J., Young, D. T., Waite, J. H. Jr., Nordholt, J. E., Thomsen, M. F., McComas, D. J., Berthelier, J. J., Williamson, W. S., Robson, R. and Mozer, F. S.: High-altitude observations of the polar wind, *Science*, 277, 349–351, 1997.

Moore, T. E., Chandler, M. O., Chappell, C. R., Comfort, R. H., Craven, P. D., Delcourt, D. C., Elliott, H. A., Glies, B. L., Horwitz, J. L., Pollock, C. J. and Su, Y.-J.: *Polar/TIDE Results on Ion Outflow*, in *Physics of Sun-Earth Plasma and Field Processes* (edited by Burch, J. L., Carovillano and Antiochos, S.), *Geophysical Monograph*, Am. Geophys. Uion, Washington, DC, 1999.

Nagai, T., Waite, J. H. Jr., Green, J. L., Chappell, C. R., Olsen, R. C. and Comfort, R. H.: First measurements of supersonic polar wind in the polar magnetosphere, *Geophys. Res. Lett.*, 11, 669–, 1984.

Nilsson, H., Joko, S., Lundin, R., Rème, H., Sauvaud, J.-A., Dandouras, I., Balogh, A., Carr, C., Kistler, L. M., Klecker, B., Carlson, C. W., Bavassano-Cattaneo, M. B., and Korth, A.: The structure of high altitude $O^+$ energization and outflows: a case study, *Ann. Geophys.*, 22, 2497–2506, 2004.

Norqvist, P., André, M., Eliasson, L., Eriksson, A. I., Blomberg, L., Lühr, H. and Clemmons, J. H.: Ion cyclotron heating in the dayside magnetosphere, *J. Geophys. Res.*, 101, 13179–, 1996.

Norqvist, P., André, and Tyrland, M.: A statistical study of ion energization mechanisms in the auroral region, *J. Geophys. Res.*, 103, 23459–23473, 1998.

Øieroset, M., Yamauchi, M., Liszka, L., and Hultqvist, B.: Energetic ion outflow from the dayside ionosphere: Categorization, classification, and statistical study, *J. Geophys. Res.*, 104, 24915–24927, 1999.

Olsen, R. C., Chappell, C. R. and Burch J. L.: Aperture plane potential control for thermal ion measurement, *J. Geophys. Res.*, 91, 3117–, 1986.

Parks, G. K.: *Physics of Space Plasma, An Introduction*, The Advanced Book Program, Addisson-Wesley Publishing Company, U.S.A., 1991.

Peterson, W. K., Collin, H. L., Doherty, M. F. and Bjørklund, C. M.: $H^+$ and $He^+$ restricted and extended (Bi-Modal) ion conic distributions, *Geophys. Res. Lett.*, 19, 1439–, 1992.

Roth, I. and Hudson, M. K.: Lower hybrid heating of ionospheric ions due to ion ring distributions in the cusp, *J. Geophys. Res.*, 90, 4191–4203, 1985.

Sauvaud, J.-A., Fontaine, D., Paschmann, G., Balogh, A., Fazakerley, A. N., and Rème, H.: A multi-instrument study of polar cap outflowing plasma, *AGU Fall Meeting 2003*, abstract#SM11C-1173, 2003.

Schunk, R. W.: Theoretical developments on the causes of ionospheric outflow, *J. Atmos. and Sol.-Terr. Phys.*, 62, 399–420, 2000.

Seki, K., Hirahara, M., Terasawa, T., Shinohara, I., Mukai, T., Saito, Y., Machida, S., Yamamoto, Y., and Kokubun, S.: Coexistence of Earth-origin $O^+$ and solar wind-origin $H^+$/$He^{++}$ in the distant magnetotail, *Geophys. Res. Lett.*, 23, 985–988, 1996.

Seki, K., Hirahara, M., Terasawa, T., Mukai, T, Saito, Y., Machida, S., Yamamoto, T., and Kokubun, S.: Statistical properties and possible supply mechanisms of tailward cold $O^+$ beams in the lobe/mantle regions, *J. Geophys. Res.*, 103, 4477–4490, 1998a.

Seki, K., Terasawa, T, Hirahara, M. and Mukai, T: Quantification of tailward cold $O^+$ beams in the lobe/mantle regions with Geotail data: Constraints on polar $O^+$ outflows, *J. Geophys. Res.*, 103, 29371–29381, 1998b.

Sharp, R. D., Johnson, R. G., and Shelley, E. G.: Observations of an ionospheric acceleration mechanism producing energetic (keV) ions primarily normal to the geomagnetic field direction, *J. Geophys. Res.*, 82, 3324–, 1977.

Sharp, R. D., Carr, D. L., Peterson, W. K. and Shelley, E. G.: Ion streams in the magnetotail, *J. Geophys, Res.*, 86, 4639–, 1981.

Shelley, E. G., Johnson, R. G., and Sharp, R. D.: Satellite observations of energetic heavy ions during a geomagnetic storm, *J. Geophys. Res.*, 77, 6104–, 1972.

Shelley, E. G., Sharp, R. D. and Johnson, R. G.: Satellite observations of an ionospheric acceleration mechanisms, *Geophys. Res. Lett.*, 3, 645–, 1976a.

Siebert, M.: *Maßzahlen der erdmagnetischen Aktivität* in *Handbuch der Physik*, vol.49/3, 206–275, Springer, Berlin Heidelberg, 1971.

Strangeway, R. J., Russell, C. T., Carlson, C. W., McFadden, J. P., Ergun, R. E., Temerin, M., Klumpar, D. M., Peterson, W. K., and Moore, T. E.: Cusp field-aligned currents and ion outflows, *J. Geophys. Res.*, 105, 21129–21142, 2000.

Su, Y.-J., Horwitz, J. L., Moore, T. E., Chandler, M. O., Craven, P. D., Glies, B. L., Hirahara, M. and Pollock, C. J.: Polar wind survey with TIDE/PSI suite aboard POLAR, *J. Geophys. Res.*, 103, 29305–, 1998.

Su, Y.-J., Ergun, R. E., Carlson, C. W., and Strangeway, R. J.: Cusp electron and ion structures observed by FAST, *AGU Fall Meeting 2002*, abstract#SM12B-11, 2002.

Sundkvist, D., Vaivads, A., André, M., Wahlund, J.-E., Hobara, Y., Joko, S., Krasnoselskikh, V. V., Bogdanova, Y. V., Buchert, S. C., Cornilleau-Wehrlin, N., Fazakerley, A., Hall, J.-O., Rème, H., and Stenberg, G.: Multi-spacecraft determination of wave characteristics near the proton gyrofrequency in high-altitude cusp, *Ann. Geophys.*, 23, 983–995, 2005.

Temerin, M.: Evidence for a large bulk ion conic heating region, *Geophys. Res. Lett.*, 13, 1059–, 1986.

Tung, Y., Carlson, C. W., McFadden, J. P., Parks, G. K., Lund, E. J., Eriksson, S., and Ergun, R. E.: Composition of auroral polar cap boundary ion conics, *AGU Fall Meeting 2002*, abstract#SM22A-0562, 2002.

Wahlund, J.-E., Eriksson, A. I., Holback, B., Boehm, M. H., Bonnell, J., Kintner, P. M., Seyler, C. E., Clemmons, J. H., Eliasson, L., Knudsen, D. J., Norqvist, P. and Zanetti, L. J.: Broadband ELF plasma emissions during auroral energization, 1, slow ion acoustic waves, *J. Geophys. Res.*, 103, 4343–, 1996.

Waite, J. H. Jr., Lockwood, M., Moore, T. E., Chandler, M. O., Horwitz, J. L. and Chappell, C. R.: *Solar Wind Control of the Geomagnetic Mass Spectrometer*, in *Solar Wind-Magnetosphere Coupling* (edited by Kamide, Y. and Slavin, J. A.), Terra Scientific, Tokyo, pp706–, 1986.

Winglee, R. M.: Mapping of ionospheric outflows into the magnetosphere for varying IMF conditions, *J. Atmos. and Sol.-Terr. Phys.*, 62, 527–540, 2000.

Wu, J., Blanc, M., Alcaydé, D., Barakat, A. R., Fontanari, J., Blelly, P.-L. and Kofman, W.: Observations of the structure and vertical transport of the polar upper ionosphere with the EISCAT VHF radar: 2. First investigations of the topside $O^+$ and $H^+$ vertical ion flows, *Ann. Geophys.*, 10, 375–, 1992.

Yau, A. W., Whalen, B. A., Peterson, W. K. and Shelley, E. G.: Distribution of upflowing ionospheric ions in the high-altitude polar cap and auroral ionosphere, *J. Geophys. Res.*, 89, 5507–, 1984.

Yau, W. A., Whalen, B. A., Abe, T., Mukai, T., Oyama, K. I. and Chang, T.: Akebono observations of electron temperature anisotropy in the polar wind, *J. Geophys. Res.*, 100, 17451–, 1995.

Yau, A. W. and André, M.: Sources of ion outflow in the high latitude ionosphere, *Space Science Rev.*, 80, 1–, 1997.

# Index